RESEARCH PROGRAM ON NEW PEROVSKITE LASER HOST MATERIALS OF THE $A[B'_{0.5}B''_{0.5}]O_3$-TYPE HAVING CUBIC CENTROSYMMETRIC LATTICE SITES

PREPARED BY
F. S. GALASSO
G. K. LAYDEN
D. E. FLINCHBAUGH

SEMI-ANNUAL REPORT
JANUARY 1965

PREPARED UNDER CONTRACT Nonr-4606(00)
PROJECT CODE NO. 4730 ARPA ORDER NO. 306

United Aircraft Research Laboratories
UNITED AIRCRAFT CORPORATION
EAST HARTFORD, CONNECTICUT

DISCLAIMER NOTICE

THIS DOCUMENT IS THE BEST QUALITY AVAILABLE.

COPY FURNISHED CONTAINED A SIGNIFICANT NUMBER OF PAGES WHICH DO NOT REPRODUCE LEGIBLY.

UNITED AIRCRAFT CORPORATION
RESEARCH LABORATORIES
East Hartford, Connecticut

D910269-3
Semiannual Report Under
Contract Nonr-4606(00)
August 1, 1964
through
January 31, 1965

Project Title: Research Program on New Perovskite Laser Host Materials of the $A(B'_{0.5}B''_{0.5})O_3$-Type Having Cubic Centrosymmetric Lattice Sites

Name of Contractor: United Aircraft Corporation Research Laboratories
Project Code No. 4730
ARPA Order No. 306

This research is part of project DEFENDER under the joint sponsorship of the Advanced Research Projects Agency, the Office of Naval Research, and the Department of Defense.

Reported By: F. S. Galasso
F. S. Galasso, Supervisor
Materials Synthesis Group

G. K. Layden
Senior Research Scientist

D. E. Flinchbaugh
Research Scientist

Approved By:
R. Fanti, Chief
Materials Sciences

Date: February 26, 1965

Report D910269-3

Semiannual Report Under Contract Nonr-4606(00)
for the Period August 1, 1964, through January 31, 1965

Research Program on New Perovskite Laser Host Materials

of the $A(B'_{0.5}B''_{0.5})O_3$-Type Having Cubic Centrosymmetric Lattice Sites

ARPA Order No. 306, Project Code No. 4730

TABLE OF CONTENTS

Report D910269-3

Semiannual Report Under Contract Nonr-4606(00)
for the Period August 1, 1964, through January 31, 1965

Research Program on New Perovskite Laser Host Materials of the $A(B'_{0.5}B''_{0.5})O_3$-Type Having Cubic Centrosymmetric Lattice Sites

ARPA Order No. 306, Project Code No. 4730

SUMMARY

During the first six months of the contract period, the Research Laboratories have been actively engaged in research directed toward obtaining laser host materials with structures having cubic centrosymmetric sites in which trivalent laser activating ions can be substituted. In this period, powders of perovskite-type compounds having the general formula $Ba(B^{3+}_{0.5}Ta_{0.5})O_3$ with B^{3+} = rare earth Y^{3+}, Sc^{3+} and In^{3+} ions were prepared and their structures analyzed by means of X-ray diffraction. The studies showed that the most suitable host materials for this program were $Ba(Y_{0.5}Ta_{0.5})O_3$, $Ba(Lu_{0.5}Ta_{0.5})O_3$, $Ba(Sc_{0.5}Ta_{0.5})O_3$ and $Ba(In_{0.5}Ta_{0.5})O_3$ because they had cubic unit cells and contained ions with appropriate electronic configurations. These compounds have been prepared with Cr^{3+} and Nd^{3+} doping, and the fluorescence spectra of the Nd^{3+} doped phases have been recorded and analyzed.

Studies involving flux growth of crystals also have been made during this period. In the first investigations, small, discolored crystals of $Ba(La_{0.5}Ta_{0.5})O_3$, $Ba(Gd_{0.5}Ta_{0.5})O_3$, $Ba(Lu_{0.5}Ta_{0.5})O_3$, $Ba(Sc_{0.5}Ta_{0.5})O_3$ and $Ba(Y_{0.5}Ta_{0.5})O_3$ were grown from a BaF_2 flux. More detailed studies of the BaO-$YTaO_4$-B_2O_3 system showed that small, clear single crystals of $Ba(Y_{0.5}Ta_{0.5})O_3$ could be grown from a B_2O_3 flux by slow cooling and that larger crystals could probably be grown using a modified Czochralski technique. The furnace and puller necessary to grow these larger crystals have been designed and are presently being fabricated.

INTRODUCTION

From theoretical calculations and the observation that the decay time of Cr^{3+} fluorescence increased from 3 msec when it is present in the aluminum-oxide structure to 46 msec in the nearly cubic $LaAlO_3$ perovskite structure (Ref. 1), it was concluded that fluorescing energy states with long lifetimes should be obtained in materials whose structures contain the doping ions as centers of symmetry in cubic crystallographic sites. More specifically, a laser host material should contain ions which are difficult to reduce, should have a structure with only one set of equivalent cubic centrosymmetric cation sites about the same size as the doping ion, and should contain an ion in these sites of the same valence state as the doping ion to be used so that no valence compensating ions have to be added. If an additional stipulation is made that trivalent rare earth or transition metal ions be used as the laser activating ions because of their stability, no laser host materials satisfying all of these requirements were available prior to the Research Laboratories discovery of ordering in a series of $A(B^{3+}_{0.5}Ta_{0.5})O_3$ perovskite-type compounds. It should be recognized, however, that these studies were preliminary in nature.

Under the present contract, work was initiated to prepare and re-examine these compounds by means of X-ray diffraction. The more promising compounds were doped with Cr^{3+} and Nd^{3+} so that the fluorescing lines could be recorded, identified, and the lifetimes of these fluorescing states could be measured. In addition, some preliminary experiments were directed toward learning how to prepare these compounds as doped single crystals so that more refined optical measurements could be made.

SELECTION OF LASER HOST MATERIALS

A survey was made of the various oxides in search of host materials with structures which contain cubic centrosymmetric crystallographic sites. In the selection of host materials, consideration was given to the stability of the oxides and doping ions which would be most suitable for substitution into the oxide structure.

Of the simple oxides, those with the sodium chloride and calcium fluoride structures have cubic centrosymmetric cation sites which will accept divalent and tetravalent ions respectively (Figs. 1a and 1b). While several of these oxides, such as MgO with the sodium chloride structure and ThO_2 and CeO_2 with the calcium fluoride structure are quite suitable as laser host lattices, the availability of

only a few relatively unstable divalent and tetravalent laser activating ions make them less desirable for the purposes of this study than host materials which will accept trivalent ions without the addition of other compensating ions.

The more complex spinel and perovskite structures contain cubic centrosymmetric sites which can accommodate trivalent cations of oxide materials. However, oxides with the spinel structure were not selected for this investigation because of the difficulty of introducing the trivalent doping ions in the octahedrally coordinated cation positions without any substitution in the tetrahedrally coordinated cation site as well (Fig. 1c). Substitution of doping ions in two different cation sites was felt to be less probable in ABO_3-type oxides with the perovskite structure because the A ion is usually much larger than the B ion (Fig. 1d). In $LaAlO_3$, for example, large rare earth ions have been substituted for the La^{3+} ions and the smaller Cr^{3+} ion has been substituted for Al (Ref. 2). The long lifetimes of the prominent fluorescing states in the Cr^{3+} doped $LaAlO_3$ indicate that this material may be nearly the ideal host oxide for this study except that its structure is slightly distorted.

Other possible host materials have become available as a result of the work reported in Refs. 3 and 4 which demonstrated that two ions which are different in size and charge could be placed in the B position of the perovskite structure. A recent compilation of these compounds with the general formula $A(B'_xB''_y)O_3$, where B' and B'' are two different elements with different charges, reveal that over 200 of them have been prepared in various laboratories (Ref. 5). When the ratio of the B'' ions to B' ions is two, as indicated by the formula $A(B'_{0.33}B''_{0.67})O_3$, and the B' and B'' ions are ordered, the structure obtained is one in which the cubic centrosymmetric B site is not preserved (Fig. 2a, Refs. 6 - 9). However, when the B' and B'' ions are present in equal amounts, as indicated by the formula $A(B'_{0.5}B''_{0.5})O_3$, a common ordered structure may be adopted in which the B ions alternate (Refs. 10, 11); thus the symmetry about the B site is retained (Fig. 2b). In these ordered $A(B'_{0.5}B''_{0.5})O_3$-type compounds it is most desirable for laser applications to have barium as the A ion since compounds containing barium are least distorted, and tantalum V as the B'' ion because of its resistance to reduction. The B' ion should be a trivalent ion and should not produce energy levels which would interfere with those of the doping ions. Therefore, B' should be trivalent scandium, yttrium, or lanthanum which have rare gas electronic configurations, trivalent gadolinium with half filled f shells, trivalent lutecium with completely filled f shells, or trivalent indium with completely filled d shells. On this basis, the compounds selected for initial studies under this contract were $Ba(La_{0.5}Ta_{0.5})O_3$, $Ba(Gd_{0.5}Ta_{0.5})O_3$, $Ba(Y_{0.5}Ta_{0.5})O_3$, $Ba(Sc_{0.5}Ta_{0.5})O_3$, $Ba(In_{0.5}Ta_{0.5})O_3$, and $Ba(Lu_{0.5}Ta_{0.5})O_3$.

In searching for other host materials, similar multiple substitutions were considered in the sodium chloride, calcium fluoride, and spinel structures as methods of obtaining new ordered structures containing cubic centrosymmetric sites.

However, a survey of the limited amount of literature on oxides reported to have ordered sodium chloride and spinel structures showed that the cations were distributed in such a way that the center of symmetry about the cation sites was not retained (Refs. 12, 13; Figs. 3, 4).

PREPARATION AND X-RAY ANALYSIS OF POWDER SAMPLES

Initial studies were conducted on $Ba(B^{3+}_{0.5}I_{..5})O_3$ ordered perovskite compounds containing various rare earth ions in addition to yttrium, scandium and indium as the B^{3+} ion, so that structural information and relative ionic radii could be obtained. The main emphasis, however, was placed on compounds containing La^{3+}, Gd^{3+}, Y^{3+}, Lu^{3+}, In^{3+} and Sc^{3+}, since these ions have appropriate electron configurations as discussed in the previous section.

Preparation of Perovskite-Type Phases

Powder samples of these perovskite-type compounds were prepared following the dry technique of reacting solids at high temperatures. In these preparations, the following chemicals were used: certified grade $BaCO_3$ from Fisher Scientific, reagent grade Ta_2O_5, high purity Le_2O_3, Gd_2O_3, Lu_2O_3, Sc_2O_3, Y_2O_3 and In_2O_3 from A. D. McKay, and high purity Nd_2O_3, Sm_2O_3, Dy_2O_3, Hc_2O_3, Er_2O_3, Tm_2O_3, Yb_2O_3 from Research Chemicals.

For each sample, $BaCO_3$ was mixed with the trivalent metal oxide and the tantalum pentoxide in a molar ratio of 2:1:1. The mixture was ground in an agate mortar and fired on alumina trays in a box furnace heated by Kanthal molybdenum disilicide elements. During the firing cycle the samples were taken from the furnace and reground to insure thorough mixing. It was found that the ordered perovskite phases could be obtained by firing the powders at 1100 - 1200°C, however, at these firing temperatures the samples also contained trivalent metal oxides or $Ba_5Ta_4O_{15}$ impurities. Single phases of $Ba(La_{0.5}Ta_{0.5})O_3$, $Ba(Eu_{0.5}Ta_{0.5})O_3$, $Ba(Y_{0.5}Ta_{0.5})O_3$ and $Ba(Sc_{0.5}Ta_{0.5})O_3$ have been prepared by firing at 1560°C. The compound containing indium is an exception, however, requiring a firing temperature of only 1400°C. All other compounds have been obtained sufficiently pure so that lattice parameters for the perovskite phases could be determined.

X-ray Analysis of Perovskite-Type Phases

All samples were examined by powder X-ray diffraction methods using a Philips 114.6 mm diameter camera and copper $K\alpha$ radiation. The lattice parameters were determined and diffraction line intensities were visually estimated for each compound as shown in Tables I and II. It was found that compounds containing the larger trivalent cations were distorted from cubic symmetry. The X-ray pattern of $Ba(La_{0.5}Ta_{0.5})O_3$ had an orthorhombic unit cell and the X-ray pattern of $Ba(Gd_{0.5}Ta_{0.5})O_3$ was indexed on a tetragonal cell. These data are given in Table I. The samples containing trivalent cations with sizes between those of La^{3+} and Gd^{3+} have not been obtained pure enough to identify their unit cell distortions. Perovskites containing ions smaller than gadolinium exhibit cubic symmetry (see Table II).

From Tables I, II and III it can be seen that the intensities of the ordering lines (when h, k and ℓ are odd integers) in the X-ray patterns of the perovskite phases correlate well with the differences in atomic scattering factors for the trivalent cations and Ta^{5+}. As this difference decreases, it becomes more difficult to observe ordering lines in the X-ray patterns, and where this difference is only 1 or 0 the ordering lines were not seen on the films at normal exposure times. It is felt, however, that ordering of the B ions does persist throughout the series. This conclusion is based on a number of studies at the Research Laboratories which showed that the difference in size of the B ions has to be very small before they will distribute themselves randomly in the B position of the perovskite structure.

Using a plot of $(volume)^{1/3}$ vs ionic radii of the B^{3+} ions as given by Ahrens and obtained from a study of $Ba(B^{3+}_{0.5}Nb_{0.5})O_3$-type compounds (Ref. 11), the effective radii of the trivalent ions used in this study were determined (see Fig. 5). Table IV presents the radii as determined by Ahrens, the radii as determined from unit cell data for $Ba(B^{3+}_{0.5}Nb_{0.5})O_3$-type compounds and the radii found in this study for the B^{3+} ions. Note that the agreement between these values are quite good except for that determined for Sc^{3+}. Scandium ions appear to have a much smaller effective ionic radii in these ordered perovskite-type compounds.

Preparation of Doped Perovskite-Type Phases

Of the various perovskite-type compounds with the general formula $Ba(B^{3+}_{0.5}Ta_{0.5})O_3$, and containing B^{3+} with the appropriate electron configuration, only $Ba(Y_{0.5}Ta_{0.5})O_3$, $Ba(Lu_{0.5}Ta_{0.5})O_3$, $Ba(In_{0.5}Ta_{0.5})O_3$ and $Ba(Sc_{0.5}Ta_{0.5})O_3$ were found to have cubic unit cells. These phases were doped with Cr^{3+} and Nd^{3+} ions and obtained as single phases by firing the stoichiometric mixtures at 1580 - 1650°C, except in the cases of the samples containing indium where a firing temperature of 1400°C was sufficient. Table V shows the phases prepared and the firing temperature used to prepare them.

CRYSTAL GROWTH EXPERIMENTS

Melting Behavior of $Ba(Y_{0.5}Ta_{0.5})O_3$

Initial crystal growing studies were conducted on $Ba(Y_{0.5}Ta_{0.5})O_3$. However, before attempting to grow crystals from a liquid phase, it was necessary to obtain information on the melting behavior of the compound in order to determine which of the several crystal growing techniques would be most applicable and which container materials could be used.

$Ba(Y_{0.5}Ta_{0.5})O_3$ was prepared by reacting $BaCO_3$, Y_2O_3 and Ta_2O_5 for several hours at 1600°C. An X-ray powder diffraction pattern was obtained for the material, and no extraneous lines were present. Attempts were made to measure the melting point of this material by placing a small piece (average dimension, 1/16 in.) on an electrically heated platinum strip, and sighting on the sample with an optical pyrometer. No melting of the sample was observed at the temperature at which the platinum strip fused. An iridium strip (MP = 2454°C) was substituted for the platinum and again the strip failed before any melting of the sample was observed. The last temperature reading made on the sample before the strip failed was 2200°C.

A piece of sintered $Ba(Y_{0.5}Ta_{0.5})O_3$ was then broken so that a sharp corner was obtained. This corner was heated with a propane-oxygen torch and observed with an optical pyrometer. Some liquid formation was observed at a nominal temperature about 2200°C. When the material had cooled to room temperature, the fused corner was broken off and X-rayed. The pattern of the recrystallized material indicated the presence of perovskite and a second phase which was recognized to be an isomorph of $BaTa_2O_6$ (see Appendix I). The presence of the second phase in the recrystallized material cannot be taken as an indication of incongruent melting of the perovskite, and later phase equilibrium studies in the system $BaO\text{-}YTaO_4\text{-}B_2O_3$ (Appendix I) clearly indicate the congruent melting behavior of $Ba(Y_{0.5}Ta_{0.5})O_3$. It may be assumed, however, that the stoichiometry of the melt is lost because of incongruent vaporization.

From the above observations it was concluded that laboratory techniques involving crystallization from the melt were impractical for this material. The standard Czochralski technique was eliminated because of the unavailability of a suitable container, and the Verneuil technique also was eliminated because of the difficulty of maintaining correct stoichiometry. For these reasons the flux-growth technique, using slow cooling or a modified Czochralski technique, was selected as the most practical method to pursue.

Preliminary Flux-Growth Experiments

Initial attempts to grow crystals of perovskite-type compounds of the general formula $Ba(B^{3+}_{0.5}Ta_{0.5})O_3$ were made by the slow cooling technique using a number of different fluxes. Single crystals of similar materials were obtained using this method just prior to the start of this contract. This information is presented in Appendix II.

Compositions were prepared from C.P. grade $BaCO_3$, Ta_2O_5, and the appropriate rare earth oxides. The batches were prefired to react the starting materials, and then mixed with various amounts of flux, placed in platinum crucibles, and subjected to a given temperature cycle in a resistance furnace controlled by a Thermovolt model AZR-2478 cam controller.

The batch composition, various heat treatments, and observations are given in Table VI. The best results were obtained using BaF_2 flux, from which small crystals of $Ba(La_{0.5}Ta_{0.5})O_3$, $Ba(Gd_{0.5}Ta_{0.5})O_3$, $Ba(Lu_{0.5}Ta_{0.5})O_3$, $Ba(Sc_{0.5}Ta_{0.5})O_3$, and $Ba(Y_{0.5}Ta_{0.5})O_3$ were grown. A photograph of $Ba(Y_{0.5}Ta_{0.5})O_3$ crystals is shown in Fig. 6. All of the crystals were strongly discolored, probably as the result of the incorporation of platinum, which is known to have an appreciable solubility in BaF_2. The crystals were generally found in the lower region of the crucible, primarily near the crucible walls, in a matrix fine-grained polycrystalline perovskite phase and flux. Moreover, close examination of the crystals disclosed that the great majority of them were twinned. These observations suggest that all of the perovskite had not dissolved in the flux at the soak temperature. Prior to the slow cooling portion of the temperature cycle, the condition prevailed wherein the molten BaF_2 was saturated with perovskite and in equilibrium with fine-grained perovskite that contained a number of twins. During the cooling cycle, presumably due to faster kinetics for deposition of dissolved perovskite on the twinned seeds, the latter grew at a considerably greater rate than the untwinned seeds. However, because of the relatively large number of twinned seeds, and the competition for material by the vastly larger number of untwinned seeds, none of these crystals grew to a large size. While these crystals were satisfactory for X-ray studies, they were not suitable for optical measurements.

Crystal Growth Experiments Using a BaF_2 Flux

Solubility of $Ba(Y_{0.5}Ta_{0.5})O_3$ in BaF_2

The preliminary flux growth experiments indicated that BaF_2 was saturated congruently with $Ba(Y_{0.5}Ta_{0.5})O_3$, but that apparently undissolved perovskite was present in the melts. The solubility of $Ba(Y_{0.5}Ta_{0.5})O_3$ was determined experimentally to confirm the above conclusion and to yield data to guide subsequent crystal growth runs in this system.

A 25 ml platinum crucible was filled with BaF_2 by charging and melting in a resistance furnace until the crucible was about 3/4 full. A sintered sample of $Ba(Y_{0.5}Ta_{0.5})O_3$ was placed in the crucible for the final charging. The crucible was then transferred to a vertical tube furnace, and Pt/Pt-10% Rh thermocouple was inserted into the melt. The melt was allowed to soak at constant temperature, and stirred periodically with 1/8 in. O.D. platinum tube. After various times of soak at various temperatures, the platinum tube was inserted about 1/4 in. below the surface of the melt, and a sample withdrawn for spectrochemical analysis.

The chemical analysis for Y and Ta of samples withdrawn at various temperatures are given in Table VII. The data indicate a reasonably constant ratio of about 2.5 moles of Ta per mole of Y. Such a result is inconsistent with the previous observation of congruent saturation of BaF_2 with perovskite, and may be due to the depletion of yttrium at the surface of the melt due to the higher volatility of YF_3. On the assumption that the experimental solubility data for Ta are a valid measure of the solubility of $Ba(Y_{0.5}Ta_{0.5})O_3$ in BaF_2, the solubility curve shown in Fig. 7 was drawn. The excellent agreement between the data obtained by approaching temperatures from above with the data obtained by approaching temperatures from below is an indication that equilibrium had been attained. It can be seen from Fig. 7 that at 1400°C $Ba(Y_{0.5}Ta_{0.5})O_3$ is soluble in BaF_2 only to the extent of 3.5 weight percent, thus confirming that an excess was present in the previous crystal growth runs.

Attempts to Nucleate $Ba(Y_{0.5}Ta_{0.5})O_3$ Crystals from a BaF_2 Flux

Using the solubility data shown in Fig. 7 as a guide, attempts were made to nucleate and grow $Ba(Y_{0.5}Ta_{0.5})O_3$ crystals from a BaF_2 flux.

Slow Cooling Method

Because of the steepness of the solubility curve, difficulty was anticipated in nucleating only a few crystals from an undercooled melt, an essential condition for obtaining large single crystals by this method. For this reason, a special furnace was built in which very accurate temperature control could be obtained during the cooling cycle. A Leeds and Northrup Speedomax type G program controller, in conjunction with a L. & N. Series 60 proportional control unit, and a 6 KVA General Electric saturable reactor, Model 69-6217, was used to control power to a Globar heated furnace. Temperature up to about 1550°C and cooling rates from 1 to 120°C/hr could be obtained.

A 100 ml platinum crucible was filled with 239 g of BaF_2, and 12.6 g (5 weight percent) of prereacted $Ba(Y_{0.5}Ta_{0.5})O_3$, and covered with a tight fitting lid to minimize vapor loss. The temperature profile of the furnace was determined, and the crucible positioned so that the bottom was about 20°C cooler than the top. The

furnace was then heated to 1530°C, allowed to soak at temperature for 8 hours and then cooled at 3°C/hr to 1300°C. The cooling rate was then increased to 120°C/hr and the furnace cooled to room temperature.

No crystals of sufficient size to be readily distinguished were found in the crucible. X-ray diffraction patterns of material from the upper portion of the crucible showed only BaF_2, while patterns of material from the bottom of the crucible showed BaF_2 and $Ba(Y_{0.5}Ta_{0.5})O_3$. Several additional attempts were made to nucleate and grow perovskite using this technique, but also without success. There appears to be a severe nucleation problem in this system, probably connected with the very steep solubility curve and low critical undercooling so that a great number of crystals, rather than a requisite few, precipitate on cooling at nearly the same time.

Modified Bridgman Technique Using Boron Nitride Crucibles

Because of the nucleation problem encountered in the normal slow cooling method, attempts were made to grow $Ba(Y_{0.5}Ta_{0.5})O_3$ from a BaF_2 flux by cooling a properly shaped crucible in a temperature gradient. Boron nitride crucibles were selected because long-term compatibility tests showed that BaF_2 could be contained in BN crucibles without any visible attack, and because of the ease with which it can be machined to shape. A BN crucible of the geometry shown in Fig. 8 was made and filled with 25 g BaF_2 and 1.25 g $Ba(Y_{0.5}Ta_{0.5})O_3$. It was inserted in a specially constructed chamber that permitted the crucible top to be screwed in place under vacuum. The crucible was held in a previously determined position inside a vertical tube furnace such that a temperature gradient of about 10°C per inch would exist across the crucible at elevated temperature. The furnace was heated so that the lower tip of the crucible attained a temperature of 1587°C, and after a soak period of 15 hours was cooled at a rate of 3°C/hr to 1300°C, and then cooled rapidly to room temperature.

Examination of the crucible and contents disclosed that no large oxide crystals had been grown. The flux contained many small metallic flakes, and on the flux surface similar flakes were found about 2 to 3 mm across. X-ray analyses showed these flakes to be TaB, indicating a reduction of the Ta^{5+} ions in the melt by the BN. No attempts have been made to repeat this experiment using other crucible materials.

Crystal Growth Experiments Using a B_2O_3 Flux

Because of the nucleation problems encountered using BaF_2 as a flux, it was necessary to find a more suitable flux for $Ba(Y_{0.5}Ta_{0.5})O_3$. Oxide fluxes were considered since it was assumed that the solubility would be higher and nucleation

problems would be less severe. Of the low melting oxides, PbO, Bi_2O_3, V_2O_5, and B_2O_3, the first three have cations that would enter the perovskite structure, and for this reason were eliminated. Studies were undertaken to delineate phase equilibrium in the system $BaO-YTaO_4-B_2O_3$ and the results are reported fully in Appendix I.

Slow Cooling Experiments

Quench data for the join $Ba(Y_{0.5}Ta_{0.5})O_3-B_2O_3$ were used to select crystal growth conditions. A mixture of 37.82g $BaCO_3$, 21.152g Ta_2O_5, 10.82g Y_2O_3, and 8.752g B_2O_3 (12.5 weight percent B_2O_3 on a fired basis) was mixed, pressed into pellets and fired slowly to 1000°C. The fired product was reground and melted into a 15 ml platinum crucible. The crucible was then placed in a vertical T-bar tube furnace, the power to which was controlled by a Leeds and Northrup Speedomax Type G program controller, Series 60 proportional controller, and Fincor FDGI saturable reactor. The furnace was heated to 1633°C, soaked for 10 hours, then cooled at 2°C/hr to 1410°C. At the latter temperature an attempt was made to withdraw the crucible from the furnace in order to decant the remaining liquid, but some material from the crucible had apparently been spilled onto, and reacted with, the furnace muffle and crucible support so that the crucible could not be withdrawn. The furnace was cooled to room temperature and the muffle was removed and sawed apart to remove the crucible.

Examination of the crucible and contents disclosed some colorless cubic crystals about 2 mm on edge adhering to the crucible walls above the level of the remaining charge. The crucible was immersed in boiling water to see if the matrix material was water-soluble; it was not. The crucible was then immersed in hot dilute nitric acid to see if the charge could be freed, but this treatment severly etched the cubic crystals, as well as the charge. The crystals were then broken from the crucible wall, and in the process were fractured. However, a fragment was X-rayed and proved to be $Ba(Y_{0.5}Ta_{0.5})O_3$. The charge was further etched in nitric acid to break down the matrix material. This treatment disclosed several large crystals but they were so badly etched that their morphology was no longer apparent. Furthermore, they could not be removed from the matrix by mechanical means without being fractured.

Although crystals could not be extracted from the matrix, it is apparent from this run that perovskite crystals can be nucleated and grown from the B_2O_3 flux. The X-ray data obtained from the flux grown crystal indicate that the latter has the same cell size as material reacted in the solid state from the components, and that no distortion is introduced. Also, the crystals grown from B_2O_3 in platinum crucibles are clear rather than discolored as was the case for crystals grown from the BaF_2 flux.

Transfer Across a Temperature Gradient

It is planned to attempt to grow large single crystals of the perovskites by the modified pulling technique employed by Linares (Ref. 14) in the growth of garnets. In this technique, nutrient dissolves in the hot region of a crucible and diffuses down a temperature gradient maintained across the solvent medium, and deposits on a seed at the cooler surface of the solvent. The seed is rotated and slowly withdrawn as growth occurs. In this technique the temperature profile across the solvent is critical. If the surface temperature is too low, so that the solvent there becomes critically supersaturated, spontaneous nucleation will occur resulting in polycrystalline deposition. The proper temperature difference between surface and nutrient must be determined experimentally. Some preliminary experiments involving gradient transport have been performed.

In this study, a solvent medium of composition 20 weight percent B_2O_3 was prepared, and 100 g of this was melted into a 50 ml platinum crucible using a Tocco Model P-10-328 induction unit; the crucible served as the susceptor. To this was added pieces of prefired $Ba(Y_{0.5}Ta_{0.5})O_3$ totaling 100 g. Thus, the gross composition was 10 weight percent B_2O_3. It can be seen from Fig. 20 (Appendix) that in the temperature range 1350 to about 1700°C, an excess of perovskite will be in equilibrium with liquid of compositions ranging between about 10 and 14 weight percent B_2O_3. The crucible was heated to about 1490°C and the temperature profile measured. The vertical gradient was determined by inserting a Pt/Pt-10% Rh thermocouple down the axis of the crucible to various depths in the liquid, and the surface temperature profile was obtained with an optical pyrometer. From these measurements it could be inferred that the temperature distribution in the crucible was approximately as shown in Fig. 9a. A similar temperature profile was obtained with the crucible at a temperature of about 1445°C as shown in Fig. 9b. Convection currents could be seen on the surface of the liquid that indicated the lines of flow shown on the above figures. Crystallites could be observed apparently forming at the surface and building up a polycrystalline island about the axis of the crucible. A thermocouple bead was held just in the surface of the liquid, and crystallites allowed to deposit on it; these were X-rayed and determined to be $Ba(Y_{0.5}Ta_{0.5})O_3$.

A platinum cover with a $\frac{1}{4}$-in. hole in the center to permit entry of the thermocouple was fitted to the crucible to serve as a radiation shield, and the vertical temperature gradient was again measured. The surface profile could not be measured, but the temperature distribution in the crucible was inferred to be as shown in Fig. 9c. The thermocouple bead was again left just below the surface of the melt. After one hour, no material had deposited on the bead. One hour later, a small deposit had been collected.

When the surface of the melt was about 80°C cooler than the bottom of the crucible, apparently spontaneous nucleation occurred indicating that the surface was critically undercooled. When the cover was placed on the crucible, the difference in temperature between bottom and surface was reduced to about 30°C. Although a visual observation of the surface was then impossible, the long time necessary to pick up a deposit on the thermocouple beads suggests that the surface layer was not critically undercooled.

OPTICAL MEASUREMENTS

This section describes the apparatus, techniques, and some results of experimental observations of optical measurements taken on powders of doped $Ba(B^{3+}_{0.5}Ta_{0.5})O_3$-type phases. With the equipment presently available, optical absorption spectra and absorption coefficients can be obtained on clear single crystals. Fluorescence emission spectra, the line width of each prominent fluorescing line, and the lifetime of the prominent fluorescing state can be obtained on either single crystals or finely ground powders. All of these measurements may be carried out at both room temperature and liquid nitrogen temperature.

Apparatus and Procedure

The UAC Research Laboratories' Cary Model 14 spectrophotometer covers the 1860 Å to 2.65 μ spectral range with automatic range change for switching the high-intensity hydrogen lamp in the ultraviolet, a high-intensity tungsten lamp in the visible range, and a separate tungsten lamp for the infrared region. The resolving power of the Model 14 is better than 1.0 Å in the ultraviolet-visible region and better than 3.0 Å in much of the near infrared. The wavelength scale is accurate to better than 4.0 Å with a reproducibility better than 0.5 Å. The photometric circuit and signal identification system is phototube shot-noise limited to give optimum signal-to-noise ratio. This instrument employs a double monochromator consisting of a 30° fused silica prism in series with a 600 line/mm echelette grating, each with its own collimating mirrors and slit system. This combination of dispersing elements provides the high resolving power and low temperature coefficient which are available with the grating at long wavelengths and at the same time retains the high optical efficiency and low scattered light characteristic of the prism monochromator. Both halves of the monochromator operate with an aperture ratio of f/8, the focal lengths being 30 cm for the prism collimator and 40 cm for the grating collimator. The monochromator has 2-cm long slits, leading to high light gathering power.

The spectrophotometer is utilized for performing transmission, absorption, and reflectivity investigations of crystals and dielectric reflecting coatings. Its optical measurement capabilities have recently been greatly expanded. The Cary spectrophotometer has been fitted with additional apparatus to allow continuous recording of fluorescence emission spectra of crystal or powder samples. An RCA 7102 photomultiplier detector having an S-1 spectral response is used to provide the recorder signal for this mode of operation. This detector is cooled near liquid nitrogen temperature to reduce thermal noise when maximum gain is required. This allows observation of fluorescence emission from 2000 Å to 1.2 microns wavelength. A 200 watt mercury-xenon arc lamp is used as an excitation radiation source lamp. A set of multiple-dielectric interference filters, in addition to glass and liquid filters, is employed to control the band pass of the pump light.

O_3-

An additional source for use in determining average lifetimes of excited states of impurity ion electrons has been constructed. It consists of a high-pressure xenon flash lamp and power supply designed to give it peak light output for 6 microseconds and decay to less than one-third that intensity in less than a microsecond. The intensity decay of the source lamp and of the sample fluorescence line are displayed on a dual-beam oscilloscope screen. Two special dewars to cool sample materials have been designed and fabricated so that optical absorption, fluorescence, and lifetime measurements can be made at temperatures down to 77°K.

For optical absorption measurements the Cary can be used in its normal mode of operation as a double monochromator. Single crystal samples with a diameter of 5 mm or more and thickness from several millimeters to several centimeters (depending on the impurity ion concentration) can be readily investigated. The unit is calibrated to read directly in absorption units with four different scale ranges: 0-0.1, 0.1-0.2, 0-1, and 1-2. Absorption or density units are defined in terms of the transmission as the logarithm of the reciprocal transmission. The sample is ground with reasonably flat and parallel ends and is positioned so that one of the monochromator beams must pass entirely through it. An SP28 photomultiplier, a thermopile, and a lead sulfide cell serve as detectors over different portions of the spectrum. Thus the absorption bands and absorption coefficients of optical quality crystals may be easily found in the near ultraviolet, visible, and near infrared spectral regions.

Fluorescence emission spectra are obtained by front lighting the sample and detecting the selected emitted light with a cooled 7102 photomultiplier tube connected to the Cary amplifier chain. The detector is also electrostatically and magnetically shielded. The d-c excited Hanovia source arc is imaged upon the sample at angles several degrees off axis to the Cary optics and the normal of the sample face. This is accomplished by a front-surface spherical condensing mirror with a central window. Fluorescence emission which leaves essentially normal to the sample face is then collected and analyzed in the instrument.

This system is ideally suited for the use of powder samples because only the front surface is illuminated and little transmission of excitation or emitted radiation through the sample medium is required. These samples are prepared either as a compressed tablet or as an opaque coating on a glass microscope slide. A sample under observation is held in contact with an arm of a stainless steel dewar with silicon grease. Combinations of liquid, colored glass, and multiple dielectric interference filters are used to select the pump light band pass. An alternative method of selecting excitation wavelengths is to use a second monochromator system as Murphy et al do (Ref. 2). Such an arrangement was tried but the Baush and Lomb instrument used was not optically fast enough to be efficient in this application. Copper and nickel sulfate solutions have been found to be useful absorbers in the long wavelength visible and infrared.

For lifetime measurements the sample is held the same way as above, but the arc lamp is removed and an E.G. and G. FX-12 xenon flash tube is substituted in its position. It is fired at 1000-2000 volts with 1.5-6 joules input. Its output spike is very sharp, but the afterglow has about a 35 μsec duration. However, even this can be neglected in view of the much greater excited state lifetimes. The 7102 signal is then fed directly to a Tektronix 551 oscilloscope and both the decay of the source light and the decay of the sample emission at a particular wavelength setting are recorded on a Polaroid Land print. The average lifetime is then measured as the sweep time required for an intensity fall of one logarithmic decrement.

Optical Measurement Data on Powders of Perovskite-Type Phases

Preliminary data were obtained initially to check out the accuracy and reliability of the instrumentation and procedures. A set of measurements with single crystal $Al_2O_3:Cr^{3+}$ was made and compared with published results. Similar data were taken with Nd^{3+} doped barium crown glass and were also found to agree with other work (Refs. 15, 16 and 17).

The fluorescence emission data for Nd^{3+} in the first set of perovskite-type powders are summarized in Table VIII. In most instances the fluorescence lines are broad. When they overlap significantly no half-intensity point line widths are listed. The spectrophotometer tracings from which these numbers are taken are illustrated in Figs. 10 - 15 and are discussed below.

A powder sample of $Ba(Sc_{.48}Nd^{3+}_{.02}Ta_{.50})O_3$ shows the transitions $^4F_{3/2}$ to $^4I_{9/2}$ and to $^4I_{11/2}$ appearing at 0.877 and 1.060 microns, respectively, at room temperature. These prominent peaks are displayed in Fig. 10. A third peak which does not appear to belong with either of these is situated at 0.977 microns. This line grows as the sample is cooled and appears centered at 0.985

microns in Fig. 11. Although a source line is known to exist in this region, the sensitivity and filtering are adjusted so that a reference base line is obtained with a block of compacted, finely ground magnesium carbonate powder which has a reflectivity of 90% here. No reflected source peak is obtained at either temperature at the settings which produced these traces. At the lower temperature the previously mentioned transitions also appear more intense and more nearly equal in magnitude. The lower energy transition appears to shift slightly. Both figures were obtained with the same instrument settings.

In these plots of relative intensity vs wavelength, the vertical scale is actually indicating decreasing density from bottom to top. This logarithmic scale is converted to linear transmittance values in Table VIII under the heading of relative intensity and for determining half-power widths.

Figures 12 and 13 show similar spectrophotometer traces for a $Ba(Y_{.495}Nd^{3+}_{.005}Ta_{.500})O_3$ pellet sample at room and liquid nitrogen temperatures. The intensity of the 1.06 micron line for the sample with the smaller impurity ion concentration is decidedly weaker than the others.

A pellet of $Ba(Lu_{.48}Nd^{3+}_{.02}Ta_{.50})O_3$ produced the results in Figs. 14 and 15 which are plotted on an expanded scale. The peak near 0.89 micron at the warmer temperature is practically lost in the broad line centered near 0.98 micron. The entrance slit settings were different for these two traces and relative intensities cannot be directly compared. No fluorescence emission data were obtained with a sample of $Ba(In_{.48}Nd^{3+}_{.02}Ta_{.50})O_3$ at either temperature.

This study will continue with the collection of more spectral data and the determination of the dependence of lifetimes on the crystalline host characteristics and on the temperature.

FUTURE WORK

During the next period, powder samples of $Ba(Y_{0.5}Ta_{0.5})O_3$, $Ba(Lu_{0.5}Ta_{0.5})O_3$, $Ba(Sc_{0.5}Ta_{0.5})O_3$ and $Ba(In_{0.5}Ta_{0.5})O_3$ will be doped with several different concentrations of Nd^{3+} and Cr^{3+} and their optical properties will be measured with particular emphasis being placed on obtaining lifetime data. In addition, some measurements will be made on Fe^{3+} and other rare earth ion doped materials. X-ray investigations will be conducted on these samples to determine which crystallographic sites the doping ions enter.

Attempts also will be made to grow single crystals of $Ba(Y_{0.5}Ta_{0.5})O_3$ using the data obtained from the phase studies in the $BaO-YTaO_4-B_2O_3$ system as a guide.

These studies (Appendix I) show that optimum flux growth conditions for $Ba(Y_{0.5}Ta_{0.5})O_3$ are obtained for composition lying on a line between the latter composition and a point 59 weight percent BaO, 20 weight percent $YTaO_4$ and 21 weight percent B_2O_3. This composition will be used to nucleate, grow and extract $Ba(Y_{0.5}Ta_{0.5})O_3$ crystals by the slow cooling technique. A rotating crucible holder has been built and installed in a program controlled globar furnace so that the liquid phase can be poured off the crystals at the end of the slow cooling cycle. A diagram of this apparatus is shown in Fig. 16. The alumina tube extends through the furnace wall and is rotated by inserting a keyed plug into the keyway of the tube. The decanted liquid is collected in a 100 ml crucible placed below the holder. It is anticipated that crystals will be obtained which are suitable both for optical property measurements, and as seeds for pulling large crystals from the flux in a thermal gradient. For the latter process, a resistance heated gradient furnace has been built to the design shown in Fig. 17. The fine brick plug in the bottom of the furnace can be accurately positioned so that a desired temperature profile in the melt can be reproduced. The furnace is powered by a 1.5 KVA saturable reactor controlled by a West Gardsman proportional controller. Measurements are currently being conducted to determine the temperature profile in a melt for various positions of the crucible.

A crystal puller capable of pulling speeds down to 0.001 cm per hour, and rotation speeds between 60 and 600 rpm is in the design stage. In the event that suitable seed crystals are not obtained by the slow cooling technique, strontium titanite single crystals will be used.

Later studies will include attempts to grow crystals doped with the more promising laser activating ions, which will be selected using optical data obtained for powder samples.

REFERENCES

1. Ohlmann, R. C.: Bull. Am. Phys. Soc., 9, 281 (1964).

2. Murphy, J., R. C. Ohlmann and R. Mazelsky: Phys. Rev. Letters, 13, 131 (1964).

3. Roy, R.: J. Am. Ceram. Soc. 37, 581 (1954).

4. Galasso, F., L. Katz and R. Ward: J. Am. Chem. Soc., 81, 820 (1959).

5. Galasso, F.: UAC Research Laboratories Report UAR-B10, January, 1963.

6. Galasso, F., J. Barrante and L. Katz: J. Am. Chem. Soc., 83, 2830 (1961).

7. Galasso, F. and J. Pyle: J. Phys. Chem., 67, 553 (1963).

8. Galasso, F. and J. Pyle: Inorg. Chem., 2, 482 (1963).

9. Galasso, F. and J. Pyle: J. Phys. Chem., 67, 1561 (1963).

10. Steward, E. G. and H. P. Rooksby: Acta Cryst., 4, 503 (1951).

11. Galasso, F. and W. Darby: J. Phys. Chem., 66, 131 (1963).

12. Blasse, G.: Z. Anorg. Allg. Chem., 326, 44, (1963).

13. Blasse, G: J. Inorg. Nucl. Chem., 25, 136 (1963).

14. Linares, R. C.: J. Appl. Phys., 35, 433 (1964).

15. Maiman, T. H., R. H. Hoskins, I. J. D'Haenens, C. K. Asawa and V. Evtuhov: Phys. Rev., 123, 1151 (1961).

16. Brown, Jr., G. C.: J. Appl. Phys., 35, 3062 (1964).

17. Snitzer, E.: Phys. Rev. Letters, 7, 444 (1961).

18. Levin, E. M. and H. F. McMurdie: J. Research Natl. Bur. Standards, 42, 131 (1949).

REFERENCES (cont'd)

19. Ferguson, R. B.: Can. Min., 6, 72 (1957).

20. Galasso, F., L. Katz and R. Ward: J. Am. Chem. Soc., 81, 5898 (1959).

21. Magneli, A. and B. Blomberg: Acta Chem. Scand. 5, 372 (1951).

22. Galasso, F. and L. Katz: Acta Cryst., 14, 647 (1960).

23. Smolenskii, G. A., V. A. Isupov and A. I. Agranovskaya: Soviet Phys. Solid State, 1, 150 (1959).

24. Smolenskii, G. A., A. I. Agranovskaya, S. N. Popov and V. A. Isupov: Soviet Phys. Tech. Phys., 3, 1981 (1958).

25. Smolenskii, G. A., A. I. Agranovskaya, V. A. Isupov: Soviet Phys. Solid State, 1, 907 (1959).

26. Remeika, J. P.: J. Am. Chem. Soc., 78, 4259 (1956).

27. Nielsen, J. W.: J. Appl. Phys., 31, 51s (1960).

APPENDIX I

PHASE EQUILIBRIA IN THE TERNARY SYSTEM $BaO-YTaO_4-B_2O_3$

Preliminary evaluation of B_2O_3 as a candidate flux for $Ba(Y_{0.5}Ta_{0.5})O_3$ indicated that the perovskite type compound has a primary phase region on the join $Ba(Y_{0.5}Ta_{0.5})O_3-B_2O_3$ existing at temperatures above approximately 1350° C, and indicated that for some unknown compositions in the quaternary system $BaO-Y_2O_3-Ta_2O_5-B_2O_3$, the primary phase region must extend as low as 1000° C. Because of the advantages to be gained by crystal growth from a flux at the lower temperatures, systematic studies of phase equilibria were undertaken to delineate the primary phase region on the plane $BaO-YTaO_4-B_2O_3$.

Preparation and Experimental Techniques

Compositions were prepared from reagent grade barium carbonate, yttrium and tantalum oxides, and anhydrous B_2O_3. For each mixture, the calculated amounts of the components were ground together under acetone, dried, and pressed into pellets. The pellets then were heated slowly and held for several hours below the melting point of B_2O_3; the temperature was then increased to a final temperature below the solidus, in most cases about 900° C. For compositions along the join $BaO-YTaO_4$, the pellets were heated rapidly to 1450° C and held 6 hours, then normally cooled and X-rayed.

The furnace used in most of the quench runs was a Globar heated vertical tube furnace. Temperature was maintained to within 2 degrees of the desired temperature by a Honeywell Pyr-o-Vane controller. For quenches from temperatures above 1400° C, a cylindrical T bar heated furnace controlled by a saturable reactor power supply and Leeds and Northrup program controller was used. The quenching apparatus consisted of a length of four-hole aluminum thermocouple tubing: the leads of a Pt/Pt-10% Rh thermocouple passed through two of the holes, and lengths of 20-mil Pt-10% Rh wire passed through the remaining holes. The upper ends of the latter wires were connected across an auto-transformer, and a short length of 10-mil platinum wire was affixed across lower ends and supported the quench envelope. When it was desired to quench the sample, a current was sent through the 10-mil platinum wire, which fused, letting the quench envelope fall into a beaker of water or mercury.

One end of a 5/8-in. length of 3 mm platinum tubing was crimped shut and folded back. The desired prereacted composition was loaded into the tube, and the top similarly crimped: a short length of Pt wire was crimped in place when

the top was folded down, and fastened to a small aluminum grommet through which passed the fuse of the quench apparatus. Thus the quench sample was within 0.25 inch of the read-out thermocouple.

In instances where there was considerable liquid formed at the quench temperature, some leakage would frequently occur from the quench packet. For this reason, in the higher temperature runs the packets were evacuated and welded shut in an electron beam welding apparatus.

The samples from the quench runs were ground in an agate mortar, and examined under the petrographic microscope. The indices of refraction of glasses, and of glasses in equilibrium with primary crystals, were measured by the oil immersion technique. X-ray powder camera diffraction photographs also were obtained on quench samples for crystalline phase identification.

The phases present and indices of refraction of glasses for various mixtures at various temperatures as determined by examination of quenched samples are recorded in Table IX.

Mixtures which contained less than about 15 percent B_2O_3 could not be quenched to clear glasses because of rapid devitrification, but always showed the presence of fine quenching crystals, as shown in Fig. 18. A similar phenomena was reported by Levin and McMurdie (Ref. 18) in the system $BaO-B_2O_3$. The presence of quenching crystals in the glass makes the index measurements unreliable. However, these quenching crystals are readily distinguished from primary crystals in the glass as shown in Fig. 19.

The Primary Phases Bounding the Perovskite Field

$YTaO_4$

Ferguson (Ref. 19) synthesized $YTaO_4$ by arc fusion at about 2100° C, and gave the indexed X-ray pattern shown in Table X. $YTaO_4$ prepared in this laboratory by solid state reaction at 1400°C is similar to Ferguson's pattern, but shows some additional lines. Furthermore, $YTaO_4$ grown as primary crystals in a B_2O_3 flux at 1015° C (sample 64-331ℓ, in Table IX) and at 1368° C (sample 65-015a) shows the same X-ray pattern as that obtained from the 1400°C solid state reaction. For this reason it is unlikely that the additional lines in the lower temperature pattern are due to a second phase or to impurities, and it is tentatively concluded that $YTaO_4$ exists in a high temperature and a low temperature modification, with the lower temperature form displaying a lower symmetry.

$BaTa_2O_6$ - Derived Solid Solutions (α Phase)

Galasso, Katz and Ward (Ref. 20) prepared $BaTa_2O_6$ by reacting $BaCO_3$ and Ta_2O_5 at 1100° C, and showed that it was isomorphous with the tetragonal tungsten bronzes (Ref. 21), having parameter a = 12.60 Å and c = 3.95 Å. They also showed that this compound could be prepared with a considerable oxygen deficiency, thus indicating a broad homogeneity range for the structure.

The X-ray data for compositions along the join $BaO-YTaO_4$ (Table IX, samples 64-322, 323, 324, and 325) indicates that a phase isomorphous with $BaTa_2O_6$ occurs at compositions around 88 weight percent $YTaO_4$. It may be assumed that this composition is simply a member of a solid solution continuum extending from $BaTa_2O_6$ out into the ternary diagram $BaO-Y_2O_3-Ta_2O_5$ but as yet no attempt has been made to accurately define the homogeneity region of solid solution in this ternary system. The lattice parameters of the solid solution in equilibrium with perovskite and liquid at 1025° C calculated from the X-ray data for sample 64-365e were found to be a = 12.68 Å and c = 4.00 Å, indicating that the cell size is increased with yttrium in solid solution.

$Ba_5Ta_4O_{15}$ (β Phase)

Galasso and Katz (Ref. 22) prepared $Ba_5Ta_4O_{15}$ and found it to belong to the trigonal system, the axes of the hexagonal unit cell being a = 5.79 Å and c = 11.75 Å. Anion deficiency could be produced by preparing the compound with tetravalent tantalum, thus indicating a considerable homogeneity range. A phase isomorphous with $Ba_5Ta_4O_{15}$ was found to have a narrow primary field in the system $BaO-YTaO_4-B_2O_3$. The exact composition of this phase is not known, although it may be assumed to be essentially $Ba_5Ta_4O_{15}$ with perhaps some Y_2O_3 in solution. However, unlike the bronze solid solution, the homogeneity region of the β phase does not extend to the $BaO-YTaO_4$ join: its occurrence as a primary phase in the system $BaO-YTaO_4-B_2O_3$ attests to the non-ternary behavior of this system.

$Ba_3B_2O_6$

Levin and McMurdie (Ref. 18) show $Ba_3B_2O_6$ to be the primary phase in the system $BaO-B_2O_3$ in mixtures containing about 78 to 87 percent BaO. According to the above authors, $Ba_3B_2O_6$ hydrates and carbonates rapidly when left in air: a sample exposed overnight to a relative humidity above 90% gave the X-ray pattern of $BaCO_3$. In the current experiments X-ray photographs were taken promptly after quenching the samples into mercury, and patterns for samples 65-016a, 016b, 017a, and 028a included the seven or eight strongest reflections for $Ba_3B_2O_6$ as reported by Levin and McMurdie, and no reflections that could be attributed to either $BaCO_3$ or $Ba(OH)_2$.

BaO

The evidence for assigning BaO as an equilibrium crystalline phase in two of the quench runs was indirect. Samples of composition 70 weight percent BaO, 20 weight percent $YTaO_4$ quenched from 1380 and 1300°C (sample 65-016a and b respectively) showed X-ray patterns for perovskite and $Ba_3B_2O_6$ only. However, the material had a strong lavender discoloration indicative of reaction of free BaO with the platinum quench packet*, whereas samples close in composition to samples 65-016a and b (e.g. samples 65-017a and 65-028a) showed no such discoloration.

Phase Equilibrium Diagram

Figures 20, 21 and 22 show the equilibrium diagrams, constructed from data in Table IX, for portions of the perovskite -B_2O_3, perovskite -BaB_8O_{13}, and perovskite-BaB_2O_4 joins respectively. Where possible, the data for the indices of refraction of glasses in equilibrium with primary crystals have been used in drawing the liquidus curves. All three of the above joins are non-binary, since phases appear which cannot be expressed in terms of the two components. Figure 23 is a map showing the primary crystallization of all the quenched compositions. Figure 24 is a projection of the liquidus surface for a portion of the system BaO-$YTaO_4$-B_2O_3 in the neighborhood of the perovskite field, constructed so as to be consistent with all the data of Table IX, using Figs. 20, 21, and 22 as guides to drawing the isotherms. The diagram indicates non-ternary equilibrium.

The data are insufficient to definitely fix the boundary curve between the fields of β and $Ba_3B_2O_6$, which could be drawn either to the left or to the right of the composition 65 weight percent BaO, 20 weight percent $YTaO_4$; the boundary curve was drawn to the left on the basis of a greater intensity of β X-ray reflections than of $Ba_3B_2O_6$ reflections from sample 65-017a.

The composition of eutectics indicated between BaO and perovskite, and between perovskite and $YTaO_4$, and consequently, the position of the boundary curves between the primary fields of BaO and perovskite and between perovskite and $YTaO_4$ were drawn arbitrarily, although with regard for the tracking of isotherms.

---

*The reaction of BaO with platinum has been reported frequently in the literature, see, for example, Ref. 18.

An interesting feature of the diagram is the fact that the primary field of the $BaTa_2O_6$ solid solution (α Phase) pinches off before intersecting the BaO-$YTaO_4$ join. This implies that yttrium substituted $BaTa_2O_6$ decomposes to perovskite and fergusonite at some temperature above at least 1400°C, but below the liquidus.

Optimum Conditions for Flux-Growth of Perovskite

In general, flux growth of single crystals of a given phase is most easily accomplished in the region of a phase diagram where the primary crystals are in equilibrium with only liquid over the greatest possible practical temperature range, and where the liquidus surface is not too steep. Since, as a melt of a given composition is cooled and primary crystallization occurs, the composition of the remaining liquid in equilibrium with crystals changes along a straight line drawn through the original composition directly away from the composition that is crystallizing out of the liquid, the obvious choice of compositions in a ternary diagram will lie on a straight line drawn from the primary crystal composition to the lowest melting four-phase equilibrium point. It can be seen from Fig. 23 that this condition is obtained for compositions along a line between perovskite and the reaction point involving perovskite, α, β, and liquid, which has the approximate composition 59 weight percent BaO, 20 weight percent $YTaO_4$ and 21 weight percent B_2O_3.

APPENDIX II

PREPARATION OF SINGLE CRYSTALS OF COMPLEX PEROVSKITE FERROELECTRIC AND SEMICONDUCTING COMPOUNDS

F. Galasso and W. Darby

(Published in Inorganic Chemistry, 4, 71 (1965))

Preparation of Single Crystals of Complex Perovskite Ferroelectric and Semiconducting Compounds

Francis Galasso and Wilda Darby
United Aircraft Corporation
Research Laboratories
East Hartford, Connecticut

SUMMARY

Single crystals of ferroelectric perovskite-type compounds with the general formula $Pb(B'_{0.5}B''_{0.5})O_3$ where B′ is scandium or iron and B″ is niobium or tantalum, and single crystals of some new semiconducting perovskite-type compounds with the general formula $La(B'_{0.5}B''_{0.5})O_3$ where B′ is a divalent ion and B″ is ruthenium or iridium were prepared from a flux and characterized by means of X-ray diffraction. Resistivity versus temperature measurements made on crystals of two of the compounds, $La(Ni_{0.5}Ru_{0.5})O_3$ and $La(Mg_{0.5}Ru_{0.5})O_3$, showed that they exhibited typical semiconductor behavior with conduction activation energies of .120 ev and .046 ev, respectively.

INTRODUCTION

Several years ago a large number of new complex compounds which contained two B elements of different valence states in the octahedrally coordinated position of the perovskite structure were prepared and studied by means of X-ray diffraction (Refs. 3, 4). In Ref. 3, these compounds were reported as a new group of structurally related materials with good potential electronic application. A recent survey of compounds of this type, however, has revealed that although over two hundred of them have been prepared to date, the electrical properties of only a few compounds have been investigated. In addition, most of these studies were made on powder compacts whose properties often are dependent on the conditions of preparation. As a consequence, investigations were initiated at the United Aircraft Research Laboratories on the preparation of single crystals

of complex perovskite-type compounds with two ions in the B position. The studies, which are reported in this paper, have resulted in the preparation of single crystals of complex ferroelectric compounds prepared previously as powders and also of single crystals of several low-resistance complex perovskite-type compounds.

EXPERIMENTAL STUDY

Ferroelectric Perovskite Compounds

The first investigations were directed towards the preparation of single crystals of four complex perovskite-type compounds whose compositions can be represented by the general formula $Pb(B'_{0.5}B''_{0.5})O_3$ where B' is scandium or iron and B'' is niobium or tantalum. These compounds were of particular interest because they were reported as having ferroelectric properties. Their Curie temperatures, which were measured on powder compacts, are reported in Table XI.

The techniques used for crystal growth were similar to either Remeika's lead oxide flux (Ref. 26) or Nielsen's lead oxide-lead fluoride flux (Ref. 27) methods. The flux and all the reactants, PbO, Sc_2O_3, Fe_2O_3, Nb_2O_5 and Ta_2O_5, used to grow single crystals of $Pb(B'_{0.5}B''_{0.5})O_3$-type compounds were all reagent grade chemicals. The perovskite samples were prepared as powders and fired for several hours at 800°, mixed with the flux and then packed into platinum crucibles. Covers were put on firmly to prevent excess vaporization of the flux. The filled crucibles were placed in a platinum-13% rhodium wound furnace and held at a maximum temperature for two hours. Cooling was controlled by a Thermovolt Electronic Program Controller.

$Pb(Sc_{0.5}Nb_{0.5})O_3$ crystals were prepared from a flux-sample mixture containing 86 wt % lead oxide flux. The mixture was cooled from 1150 to 900°C at 30°/hr.

$Pb(Sc_{0.5}Ta_{0.5})O_3$ crystals were grown from a mixture containing 42.5 wt % lead oxide and 42.5 wt % lead fluoride flux. These samples were cooled from 1325° to 1025° at 25°/hr.

$Pb(Fe_{0.5}Nb_{0.5})O_3$ and $Pb(Fe_{0.5}Ta_{0.5})O_3$ crystals were prepared following Remeika's technique. These samples were cooled at 5°/hr from 1230 to 900°C. For growing crystals of $Pb(Fe_{0.5}Nb_{0.5})O_3$ and $Pb(Fe_{0.5}Ta_{0.5})O_3$, 64 wt % lead oxide was mixed with the former compound and 54 wt % lead oxide mixed with the latter, and the samples were cooled at 5°/hr from 1230 to 800°C.

The $Pb(Sc_{0.5}Nb_{0.5})O_3$, $Pb(Fe_{0.5}Ta_{0.5})O_3$ and $Pb(Sc_{0.5}Ta_{0.5})O_3$ crystals obtained using these procedures were small cubes about 1 mm on edge, while the

$Pb(Fe_{0.5}Nb_{0.5})O_3$ crystals were slightly larger and more irregular in shape. All $Pb(B'_{0.5}B''_{0.5})O_3$ crystals were dark brown in color except for crystals of $Pb(Sc_{0.5}Nb_{0.5})O_3$ which were dark blue to black. Crystal cubes of $Pb(Sc_{0.5}Ta_{0.5})O_3$ were joined together in flat sheets which seem to have grown in layers parallel to the bottom of the crucible.

X-ray precession photographs were taken of a well-formed crystal of each compound to insure that it was single. These photographs showed patterns which indicated that they had perovskite-type structures. Powder diffraction photographs of ground crystals taken using a 57.3 mm Philips X-ray camera with copper K_α radiation confirmed the single crystal diffraction data and showed no evidence of ordering of the B ions in the structure of any of the compounds. It should be noted, however, that the back reflection lines in the X-ray powder pattern of $Pb(Sc_{0.5}Nb_{0.5})O_3$ were broad, which may mean that its unit cell is slightly distorted from the one found in the ideal cubic perovskite structure, or that the crystal was not uniform in composition. The unit cell sizes for the $Pb(B'_{0.5}B''_{0.5})O_3$-type compounds are given in Table XI. These must be presumed to be cell parameters of the cubic pseudocells, even though the splitting of back reflection lines could not be detected because ferroelectric crystals cannot be perfectly cubic.

Semiconducting Perovskite Compounds

Attempts also were made to prepare a number of new perovskite-type compounds with the general formula $La(B'_{0.5}B''_{0.5})O_3$ where B' is a divalent ion and B'' is Ru or Ir in a single crystal form. These black compounds were produced initially as powders at the Research Laboratories by mixing reagent grade La_2O_3, a divalent metal oxide, and RuO_2 or IrO_2 in a 1:1:1 molar ratio and firing the mixture in air at 1150° for 24 hr. These materials were of interest because of their low electrical resistances and stability in air.

Single crystals of four of the $La(B'_{0.5}B''_{0.5})O_3$-type compounds were prepared using either a lead oxide or a lead oxide-lead fluoride flux with enough La_2O_3, a divalent metal oxide, and RuO_2 or IrO_2 to form the desired compound (Refs. 26, 27). The flux techniques employed were similar to those used to grow the $Pb(B'_{0.5}B''_{0.5})O_3$-type crystals. The amount and composition of the fluxes, firing conditions, and cooling rates are given in Table XII. The resulting black crystals were cubic in shape.

X-ray powder diffraction photographs, taken of the powders and ground crystals, showed the typical perovskite pattern with extra lines. However, the entire diffraction pattern of these compounds still could be indexed on the basis of a cubic unit cell with an edge twice the length of the simple perovskite cell "a" axis. A typical indexing, in this case, for $La(Ni_{0.5}Ru_{0.5})O_3$, is given

in Table XIII and the unit cell sizes for all of the $La(B'_{0.5}B''_{0.5})O_3$-type compounds prepared in this study are given in Table XIV. The cell sizes observed indicate that magnesium and zinc both have larger effective ionic radii than nickel. The fact that the magnesium ions appear to be larger than the nickel ions is consistent with the results obtained for ordered $A(B'_{0.33}Nb_{0.67})O_3$ perovskite-type compounds (Ref. 9). The much smaller cell size found for compounds which contain manganese, however, probably means that the manganese is in the trivalent state. It should be noted that the lattice type for these compounds is simple cubic and not face-centered cubic as it is for the ordered $Ba(B'_{0.5}Nb_{0.5})O_3$ perovskite-type compounds prepared in a previous study (Ref. 11). Precession X-ray photographs of the single crystals showed diffraction symmetry to be m3m and a systematic absence of hOO reflections when h is odd. Therefore, the crystals probably belong to the space group $P4_232$.

Although the low resistances of all of these compounds were confirmed by single measurements, only the single crystals of two of them, $La(Ni_{0.5}Ru_{0.5})O_3$ and $La(Mg_{0.5}Ru_{0.5})O_3$, were found to be sufficiently large and well-shaped so that platinum paste electrodes could be applied to the faces and extensive electrical resistivity measurements made. The former cubic crystals were 2 mm on an edge while the latter were 1 mm on an edge. A constant current was applied and the voltage drop was measured across a standard resistor in series with the crystal. The plots of log resistivity versus 1000/T for $La(Ni_{0.5}Ru_{0.5})O_3$ and $La(Mg_{0.5}Ru_{0.5})O_3$ shown in Fig. 25 are typical of semiconductors. Calculations from these plots show that the conduction activation energies for these compounds are .120 ev and .046 ev, respectively.

CONCLUSIONS

The growth of single crystals of several complex perovskite-type compounds, although the crystals are not large, is a step toward obtaining many of these materials in a suitable form for good electrical measurements. Crystals of $La(Ni_{0.5}Ru_{0.5})O_3$ and $La(Mg_{0.5}Ru_{0.5})O_3$, for instance, were large enough to make meaningful resistivity measurements. It is realized that other techniques of crystal growing besides the flux technique may produce larger crystals of complex perovskite-type compounds. In this connection, investigations of growing these crystals by the Czochralski and Verneuil techniques are presently being conducted at the Research Laboratories.

ACKNOWLEDGMENT

The authors wish to thank Bernarr Jacob and Valentine Patarini for their assistance in crystal growing and making electrical measurements.

LIST OF TABLES

TABLE I

X-ray Data for Distorted, Ordered Perovskite-Type Compounds

$Ba(La_{0.5}Ta_{0.5})O_3$ a_o=8.611, b_o=8.639, c_o-8.764 Å			$Ba(Gd_{0.5}Ta_{0.5})O_3$ a_o= 8.487, c_o= 8.513 Å		
hkl (obs.)	d obs., Å	I/Io	hkl (obs.)	d obs., Å	I/Io
111	5.00	40	111	4.90	30
200,020	4.32	40	200	4.25	30
220	3.05	100	220	3.00	100
311	2.60	30	311	2.555	20
222	2.50	10	222	2.450	10
400,040	2.159	70	400	2.122	70
420	1.925	20	420	1.894	10
422	1.761	80	422	1.732	90
333	1.668	20	440	1.501	60
404	1.535	30	620	1.341	70
440	1.525	60	444	1.225	50
260	1.365	60	642	1.134	70
444	1.253	20	800	1.060	20
326	1.247	30	822,660	0.999	40
264,624	1.159	40	408	0.950	20
462,642	1.154	70	840	0.948	40
080	1.080	30	646	0.906	30
800	1.076	30	448	0.868	30
308	1.024	60	844	0.866	40
822	1.016	60	2,0,10	0.834	30
840	0.964	40	10,2,0	0.832	80
508	0.924	30	4,2,10	0.777	50
805	0.918	40	10,2,4	0.775	80
409	0.887	20			
484	0.883	20			
844	0.882	30			
10,1,1	0.852	20			
0,10,2	0.847	40			
10,0,2	0.845	70			
1,0,11	0.793	20			
1,1,11	0.790	20			
4,10,2	0.789	30			
10,4,2	0.787	30			
0,11,0	0.785	40			
11,0,0	0.783	20			

TABLE II

X-ray Data for Cubic, Ordered Perovskite-Type Compounds

	$Ba(Dy_{0.5}Ta_{0.5})O_3$ a_o = 8.454 Å		$Ba(Ho_{0.5}Ta_{0.5})O_3$ a_o = 8.442 Å		$Ba(Y_{0.5}Ta_{0.5})O_3$ a_o = 8.433 Å	
hkl	d_{obs} Å	I/I_o	d_{obs} Å	I/I_o	d_{obs} Å	I/I_o
111	4.88	30	4.88	40	4.88	50
200	4.22	30	4.22	30	4.24	20
220	2.98	100	2.98	100	2.98	100
311	2.544	10	2.544	20	2.543	30
222	2.445	10	2.438	10	2.430	20
400	2.113	90	2.109	80	2.108	70
331			1.934	10		
420	1.887	20				
422	1.725	90	1.721	90	1.722	80
511,333			1.622	10	1.624	20
440	1.495	60	1.491	70	1.491	60
531			1.426	40	1.424	20
600,442			1.409	30		
620	1.337	70	1.335	70	1.335	60
622						
444	1.220	50	1.219	30	1.217	40
711,551			1.183	10		
640						
533						
642	1.130	80	1.127	80	1.127	70
731,553						
800	1.057	30	1.054	30	1.053	20
733						
820,644						
822,660	0 998	50	0.994	70	0.994	50
751,555						
662						
840	0.945	40	0.944	60	0.942	50
911,753						
664	0.901	40	0.900	60	0.899	30
931						
844	0.863	50	0.861	70	0.860	40
933,755,771						
10,0,0						
10,2,0;862	0.829	80	0.828	90	0.827	70
951,773						
10,2,2						
953			0.787	10		
10,4,0;864						

TABLE II (cont'd)

	$Ba(Er_{0.5}Ta_{0.5})O_3$ a_o = 8.423 Å		$Ba(Tm_{0.5}Ta_{0.5})O_3$ a_o = 8.406 Å		$Ba(Yb_{0.5}Ta_{0.5})O_3$ a_o = 8.390 Å	
hkl	d_{obs} Å	I/I_o	d_{obs} Å	I/I_o	d_{obs} Å	I/I_o
111	4.86	20	4.82	< 10		
200	4.21	40	4.18	10	4.20	50
220	2.97	100	2.97	100	2.96	100
311						
222						
400	2.103	70	2.099	80	2.099	80
331						
420	1.881	20	1.879	10	1.879	30
422	1.720	90	1.711	90	1.714	90
511,333						
440	1.491	70	1.485	60	1.485	70
531						
600,442	1.404	10			1.398	20
620	1.332	70	1.329	70	1.329	70
622						
444	1.215	60	1.212	40	1.212	30
711,551						
640						
533						
642	1.125	80	1.123	80	1.121	80
731,553						
800	1.052	30			1.048	30
733						
820,644						
822,660	0.992	70	0.991	50	0.988	60
751,555						
662						
840	0.941	70	0.940	40	0.938	60
911,753						
664	0.898	60	0.897	40	0.894	50
931						
844	0.860	70	0.858	40	0.856	60
933,755,771						
10,0,0						
10,2,0;862	0.826	90	0.825	60	0.823	90
951,773						
10,2,2						
953						
10,4,0;864	0.782	20			0.779	20

TABLE II (cont'd)

	$Ba(Lu_{0.5}Ta_{0.5})O_3$ a_o = 8.372 Å		$Ba(In_{0.5}Ta_{0.5})O_3$ a_o = 8.280 Å		$Ba(Sc_{0.5}Ta_{0.5})O_3$ a_o - 8.222 Å	
hkl	d_{obs} Å	I/I_o	d_{obs} Å	I/I_o	d_{obs} Å	I/I_o
111			4.76	30	4.75	50
200	4.20	50	4.14	50	4.12	10
220	2.96	100	2.93	100	2.91	100
311			2.501	20	2.478	40
222			2.388	30	2.373	30
400	2.095	70	2.071	80	2.058	70
331					1.8[illegible]	20
420	1.869	40	1.850	40		
422	1.710	90	1.690	90	1.680	80
511,333			1.591	20	1.582	20
440	1.480	60	1.464	60	1.455	50
531			1.399	20	1.389	20
600,442	1.396	20	1.378	20		
620	1.324	60	1.308	70	1.302	50
622						
444	1.209	40	1.195	50	1.188	30
711,551					1.153	10
640						
533						
642	1.120	70	1.105	80	1.099	70
731,553					1.070	10
800	1.046	30	1.035	40	1.029	20
733						
820,644						
822,660	0.986	50	0.976	70	0.969	50
751,555						
662						
840	0.936	50	0.926	70	0.919	40
911,753						
664	0.892	40	0.882	40	0.877	40
931						
844	0.854	50	0.845	50	0.839	50
933,755,771						
10,0,0						
10,2,0;862	0.821	80	0.812	80	0.806	80
951,773					0.795	10
10,2,2						
953						
10,4,0;864	0.777	10				

TABLE III

Structure Data for $Ba(B^{3+}_{0.5}Ta_{0.5})O_3$-Type Compounds

Perovskite	Lattice Parameters, Å	Diff. in Ionic Radii of B Ions, Å *	Diff. in Atomic Scattering Factor of B Ion
$Ba(La_{0.5}Ta_{0.5})O_3$	a_o = 8.611 b_o = 8.639 c_o = 8.764	.46	14
$Ba(Nd_{0.5}Ta_{0.5})O_3$	a_o = 8.556	.35	11
$Ba(Sm_{0.5}Ta_{0.5})O_3$	a_o = 8.519	.32	9
$Ba(Eu_{0.5}Ta_{0.5})O_3$	a_o = 8.506	.31	8
$Ba(Gd_{0.5}Ta_{0.5})O_3$	a_o = 8.487 c_o = 8.513	.30	7
$Ba(Dy_{0.5}Ta_{0.5})O_3$	a_o = 8.454	.26	5
$Ba(Ho_{0.5}Ta_{0.5})O_3$	a_o = 8.442	.25	4
$Ba(Y_{0.5}Ta_{0.5})O_3$	a_o = 8.433	.24	32
$Ba(Er_{0.5}Ta_{0.5})O_3$	a_o = 8.423	.23	3
$Ba(Tm_{0.5}Ta_{0.5})O_3$	a_o = 8.406	.22	2
$Ba(Yb_{0.5}Ta_{0.5})O_3$	a_o = 8.390	.20	1
$Ba(Lu_{0.5}Ta_{0.5})O_3$	a_o = 8.372	.18	0
$Ba(In_{0.5}Ta_{0.5})O_3$	a_o = 8.280	.10	22
$Ba(Sc_{0.5}Ta_{0.5})O_3$	a_o = 8.236	.06	50

* Values for the B^{3+} ion radii as obtained in the present study. The radius used for Ta^{5+} as determined by Ahrens.

TABLE IV

Radii for Trivalent Cations

B^{3+} Ion	Radius, Å - Ahrens	From Previous UAC Study	This Study
La	1.14		1.14
Nd	1.04	1.04	1.03
Sm	1.00	1.00	1.00
Eu	.98	.99	.99
Gd	.97	.98	.98
Dy	.92	.92	.94
Y	.92		.93
Ho	.91	.91	.93
Er	.89	.91	.91
Tm	.87	.90	.90
Yb	.86	.86	.88
Lu	.85	.85	.86
In	.81	.78	.78
Sc	.81	.74	.74

TABLE V

Nd^{3+} and Cr^{3+} Doped, Ordered Perovskite-Type Compounds

Nd^{3+} Doped Compounds	Firing Temp °C
$Ba(Y_{.495}Nd^{3+}_{.005}Ta_{.500})O_3$	1600
$Ba(Lu_{.480}Nd^{3+}_{.02}Ta_{.500})O_3$	1600
$Ba(In_{.480}Nd^{3+}_{.02}Ta_{.500})O_3$	1400
$Ba(Sc_{.480}Nd^{3+}_{.02}Ta_{.500})O_3$	1600

Cr^{3+} Doped Compounds	Firing Temp °C
$Ba(Y_{.480}Cr^{3+}_{.020}Ta_{.500})O_3$	1580
$Ba(Lu_{.480}Cr^{3+}_{.020}Ta_{.500})O_3$	1600
$Ba(In_{.480}Cr^{3+}_{.020}Ta_{.500})O_3$	1600
$Ba(Sc_{.480}Cr^{3+}_{.020}Ta_{.500})O_3$	1650

TABLE VI

Preliminary Crystal Growth Runs

Composition in Weight %			Soak		Cooling Rate	Observations
	Perovskite	Flux	T °C	Hour	°C/hour	
25	$Ba(Y_{0.5}Ta_{0.5})O_3$	BaF_2	1400	1.5	9	no crystals
25	$Ba(Y_{0.5}Ta_{0.5})O_3$	$KF \cdot 2H_2O$	900	2.5	6	no crystals
16.5	$Ba(Y_{0.5}Ta_{0.5})O_3$	BaF_2	1400	7	12	yellow to orange cubic crystals $< \frac{1}{2}$ mm - x-ray, ordered perovskite
13.1	$Ba(Gd_{0.5}Ta_{0.5})O_3$	BaF_2	1400	5	7	few very small crystals
4	$Ba(Gd_{0.5}Ta_{0.5})O_3$	BaF_2	1415	15	3.5	black crystals $< \frac{1}{2}$ mm - x-ray, ordered perovskite (distorted)
8	$Ba(Lu_{0.5}Ta_{0.5})O_3$	BaF_2	1460	18	4.5	thin blue plates $< \frac{1}{2}$ mm on edge
13	$Ba(La_{0.5}Ta_{0.5})O_3$	BaF_2	1432	15	4	black, irregular shaped crystals up to 1 mm
15	$Ba(Sc_{0.5}Ta_{0.5})O_3$	BaF_2	1385	20	7	yellow crystals $< \frac{1}{2}$ mm
93	$Ba(Lu_{0.5}Ta_{0.5})O_3$	BaF_2	1385	3.5	4	no crystals
13	$Ba(In_{0.5}Ta_{0.5})O_3$	BaF_2	1385	5	4.5	no crystals
7	$Ba(In_{0.5}Ta_{0.5})O_3$	BaF_2-$BaCl_2$	1330	4	4.5	no crystals
5	$Ba(Y_{0.5}Ta_{0.5})O_3$	BaF_2	1385	20	4	no crystals
9.5	$Ba(In_{0.5}Ta_{0.5})O_3$	BaF_2	1452	15	4	no crystals
50	$Ba(Y_{0.5}Ta_{0.5})O_3$	PbO-PbF_2	1020	13	4.4	no crystals-perovskite powder has smaller cell size due to Pb substitution
8	$Ba(Gd_{0.5}Ta_{0.5})O_3$	GdF_3	1335	13	4	no crystals

TABLE VII

Solubility Data for $Ba(Y_{0.5}Ta_{0.5})O_3$ in BaF_2

Heat Treatment	Spectrochemical Analysis	
	w/o Ta	w/o Y
heat up slowly from room temperature, soak 1.5 hours at 1420°C	1.1	.21
heat up from 1420 to 1520°C, 1.5 hour soak	2.1	.38
cooled from 1520 to 1350°C, soaked 18 hours, then heated to 1610°C, soaked 1 hour	3.9	.78
cooled from 1610°C to room temperature, reheated to 1535°C, 3/4-hour soak	2.3	.38
cooled from 1535 to 1405°C, 1-hour soak	1.0	.19

TABLE VIII

Fluorescence Emission Data for Nd^{3+} in Perovskite Hosts

Compound	Prominent Line Peaks	Half Power Width	Relative Intensity	Temperature
$Ba(Sc_{.48}Nd^{3+}_{.02}Ta_{.50})O_3$	0.877 μ	500 Å	3.6%	300° K
	1.060	350	2.7	
	0.877	480	8.2	77°
	1.060		7.6	
	0.985		9.6	
$Ba(Y_{.495}Nd^{3+}_{.005}Ta_{.500})O_3$	0.895		1.3	300°
	1.060		1.7	
	0.896		2.4	77°
	1.066		2.2	
	0.980		3.4	
$Ba(Lu_{.48}Nd^{3+}_{.02}Ta_{.50})O_3$	0.893	510	3.4	300°
	1.066	430	3.0	
	0.984		8.5	77°
	1.072		2.6	

TABLE IX

Quench Data for Samples in the System $BaO-YTaO_4-B_2O_3$

Sample No.	Composition in Weight %			T °C	Phases Present
	BaO	$YTaO_4$	B_2O_3		
64-322	62.8	37.2	0	1450	P + BaO*
64-323	31.5	68.5	0	1450	P + α
64-324	23.5	76.5	0	1450	P(tr) + α
64-325	18.7	81.3	0	1450	α
64-331i	33.4	36.6	30	1345	gl η = 1.667
64-331k	33.4	36.6	30	1240	gl η = 1.669
64-331j	33.4	36.6	30	1110	gl η = 1.665
64-331ℓ	33.4	36.6	30	1015	gl η = 1.632 + $YTaO_4$
64-371a	35.9	39.1	25	1345	gl η = 1.750
64-357c	38.2	41.8	20	1390	gl η = 1.770
64-357a	38.2	41.8	20	1310	gl η = 1.770
64-357b	38.2	41.8	20	1235	gl η = 1.743 + α
64-357d	38.2	41.8	20	1160	gl η = 1.740 + α
64-374a	40.7	44.3	15	1420	gl η = 1.795
64-427d	41.8	45.7	12.5	1593	gl η ~ 1.82 + qx
64-427b	41.8	45.7	12.5	1480	gl η ~ 1.82 + qx + P(tr)
64-427f	41.8	45.7	12.5	1432	gl η ~ 1.82 + qx + P
64-427c	41.8	45.7	12.5	1368	gl η + qx + P
64-427a	41.8	45.7	12.5	1315	gl η = 1.787 + P + α (tr)
64-368g	43	47	10	1720	gl η ~ 1.83 + qx + P(tr)
64-368h	43	47	10	1557	gl η ~ 1.83 + qx + P
64-368b	43	47	10	1395	gl η ~ 1.82 + qx + P
64-368a	43	47	10	1305	gl η = 1.787+ P + α
64-368c	43	47	10	1205	gl η = 1.753+ P + α
64-368d	43	47	10	1172	gl + P + α
64-368e	43	47	10	1025	gl + P + α
64-368i	43	47	10	925	gl + P + α + β

TABLE IX(cont'd)

Sample No.	Composition in Weight %				Phases Present
	BaO	$YTaO_4$	B_2O_3	T °C	
64-314b	44	26	30	1150	gl
64-314c	44	26	30	950	gl + α
64-396	45	30	25	1200	gl η = 1.737
64-396a	45	30	25	1100	gl η = 1.725 + α (tr)
64-396b	45	30	25	1035	gl + α
64-396c	45	30	25	908	unidentified solid phases
64-411a	45.5	34.5	20	1300	gl η = 1.762
64-411b	45.5	34.5	20	1215	gl η = 1.745 + α
64-412c	46	39	15	1305	gl η = 1.780
64-412b	46	39	15	1210	gl η = 1.747 + α
64-417e	47	43	10	1470	gl η = 1.797 + P
64-417f	47	43	10	1342	gl η = 1.778 + P
64-417b	47	43	10	1315	gl η = 1.778 + P
64-417c	47	43	10	1300	gl + P + α
64-417d	47	43	10	1253	gl + P + α
64-417a	47	43	10	1145	gl + P + α
65-014a	60.5	19.5	20	1280	gl η = 1.725
65-014c	60.5	19.5	20	1049	gl η = 1.725
65-014b	60.5	19.5	20	1005	gl η = 1.725 + β (tr)
65-002e	57	28	15	1480	gl η = 1.778 + qx
65-002d	57	28	15	1360	gl η = 1.755 + P(tr)
65-002c	57	28	15	1280	gl η = 1.757 + P
65-002b	57	28	15	1193	gl η = 1.743 + P
65-002a	57	28	15	1100	gl η = 1.738 + P
65-001b	54	36	10	1106	gl η = 1.735 + P
65-001a	54	36	10	1083	gl η = 1.735 + P
65-001c	54	36	10	1050	gl η = 1.725 + P
65-001d	54	36	10	1000	gl η = 1.725 + P
65-001j	54	36	10	978	gl(tr) + P + β (tr)
65-001i	54	36	10	945	β + weak unidentified
65-001g	54	36	10	927	β + weak unidentified

TABLE IX(cont'd)

Sample No.	Composition in Weight %			T °C	Phases Present
	BaO	$YTaO_4$	B_2O_3		
65-052a	55	23	22	1055	gl + α (tr)
65-052b	55	23	22	1011	gl + α
65-016b	70	20	10	1380	P + BaO* + $Ba_3B_2O_6$
65-016a	70	20	10	1300	P + BaO* + $Ba_3B_2O_6$
65-028a	63	27	10	1300	gl + P + $Ba_3B_2O_6$ (tr)
65-017a	65	20	15	1005	gl + β + $Ba_3B_2O_6$
65-018a	50	20	30	1010	gl η = 1.685, α + β
65-015a	30	60	10	1368	gl + $YTaO_4$
65-015b	30	60	10	1295	gl + $YTaO_4$ + α
65-039a	35	50	15	1300	gl + $YTaO_4$ + α
65-051a	35	55	10	1358	gl + $YTaO_4$ + α (tr)
65-038a	39	50	11	1297	gl + P(tr) + α

TABLE IX(cont'd)

Quaternary Compositions

Sample No.	Composition in Weight %					Phases Present
	BaO	Y_2O_3	Ta_2O_5	B_2O_3	T °C	
64-389	45.25	17.5	27.5	10	1200	gl + P + α
64-394a	45.5	18.4	22.6	13.5	1200	gl + unidentified phases
64-394b	45.5	18.4	22.6	13.5	1100	gl + α + unidentified phases
64-398	45.58	17.88	26.04	10.5	1200	gl + P + unidentified

gl = glass

η = index of refraction

P = $Ba(Y_{0.5}Ta_{0.5})O_3$

α = phase isomorphous with $BaTa_2O_6$

β = phase isomorphous with $Ba_5Ta_4O_{15}$

(tr) = trace

qx = quenching crystals (see text)

*the criterion for assigning BaO as a crystalline phase is explained in the text

TABLE X

X-ray Patterns of $YTaO_4$

hkl	Ferguson* d	I/I$_o$	UAC** d	I/I$_o$
020	5.47	10	5.45	35
110	4.79	40	5.05	40
			3.78	35
			3.71	35
$\bar{1}21$	3.14	100	3.16	100
130	3.02	5		
031,121	2.94	100	2.92	100
040	2.74	40	2.72	40
200	2.64	40	2.63	40
002	2.52	30	2.54	40
			2.451	10
			2.417	30
220,$\bar{2}$11	2.38	5	2.370	1
$\bar{1}$12,022	2.30	5	2.300	7
			2.231	10
			2.191	7
112,141	2.15	30	2.143	30
			2.068	10
$\bar{2}$31,150,051	2.02	20	2.035	8
231,$\bar{2}$02	1.921	30	1.941	40
240	1.901	50	1.893	40
042	1.846	60	1.857	50
			1.822	5
			1.799	10
202,310	1.741	30	1.733	35
			1.710	40
321,$\bar{2}$51	1.639	60	1.642	50
152	1.605	20	1.611	12
			1.595	20
251,$\bar{2}$42	1.570	60	1.581	15
152	1.549	30	1.539	35
071	1.494	50	1.500	45
$\bar{2}$13	1.467	20	1.474	20

TABLE X (cont'd)

hkl	Ferguson* d	I/I$_o$	UAC** d	I/I$_o$
			1.463	20
			1.423	10
			plus many additional lines	

*Sample prepared by arc fusion at about 2100°C

**Sample reacted in the solid state at about 1400°C; also obtained as primary crystals from B_2O_3 flux at 1015°C and 1368°C.

TABLE XI

Cell Sizes and Ferroelectric Data for $Pb(B'_{0.5}B''_{0.5})O_3$-Type Compounds

Compound	Cell Size, Å *	Curie Temp., °C
$Pb(Sc_{0.5}Nb_{0.5})O_3$	4.086	90 (23)
$Pb(Sc_{0.5}Ta_{0.5})O_3$	4.080	26 (23)
$Pb(Fe_{0.5}Nb_{0.5})O_3$	4.017	112 (24)
$Pb(Fe_{0.5}Ta_{0.5})O_3$	4.011	-30 (25)

*Pseudocubic cell size

TABLE XII

Crystal Growing Data for $La(B'_{0.5}B''_{0.5})O_3$-Type Compounds

Compound	Flux	Flux: Sample Ratio wt. %	Temp. Range, °C	Cooling Rate, °/hr	Crystal Size mm edge
$La(Ni_{0.5}Ru_{0.5})O_3$	PbO	85:15	1300-850	30	0.5 max.
	$PbO \cdot PbF_2$	85:15	1300-1000	30	2
$La(Ni_{0.5}Ir_{0.5})O_3$	$PbO \cdot PbF_2$	85:15	1300-1000	30	0.5
$La(Mg_{0.5}Ru_{0.5})O_3$	$PbO \cdot PbF_2$	85:15	1320-1000	30	1
$La(Zn_{0.5}Ru_{0.5})O_3$	PbO	80:20	1300-25	50	0.1

TABLE XIII

X-ray Data for $La(Ni_{0.5}Ru_{0.5})O_3$

hkl	I/I_o	d_{obs} Å	d_{cal} Å
111	10	4.55	4.56
200	40	3.91	3.95
210	10	3.52	3.53
220	100	2.78	2.78
221	10	2.62	2.63
311	10	2.37	2.38
222	50	2.27	2.28
320	10	2.18	2.19
400	80	1.970	1.975
410	30	1.915	1.916
420	40	1.765	1.767
421	40	1.722	1.724
422	90	1.611	1.613
430	< 10	1.578	1.580
432,520	20	1.465	1.467
440	60	1.395	1.397
522,441	< 10	1.374	1.375
531	< 10	1.335	1.336
600,442	< 10	1.317	1.317
610	< 10	1.298	1.299
620	70	1.248	1.249
621,540	20	1.233	1.234
622	10	1.191	1.191
630	20	1.178	1.178
444	50	1.140	1.140
632	10	1.129	1.130
641,720	< 10	1.082	1.086
642	80	1.055	1.056
722	< 10	1.044	1.048
650	10	1.010	1.012

TABLE XIV

Lattice Parameters for $La(B'_{0,5}B''_{0,5})O_3$-Type Compounds

Compound	Cell Size, Å
$La(Ni_{0,5}Ru_{0,5})O_3$	7,90 [a]
$La(Ni_{0,5}Ir_{0,5})O_3$	7,90 [a]
$La(Mn_{0,5}Ru_{0,5})O_3$	,84 [b]
$La(Mn_{0,5}Ir_{0,5})O_3$	7,86 [b]
$La(Mg_{0,5}Ru_{0,5})O_3$	7,91 [a]
$La(Mg_{0,5}Ir_{0,5})O_3$	7,92 [b]
$La(Zn_{0,5}Ru_{0,5})O_3$	7,97 [c]

a) From X-ray data for ground single crystals

b) From single crystal X-ray data

c) From X-ray data for powder samples

LIST OF FIGURES

STRUCTURE DIAGRAMS

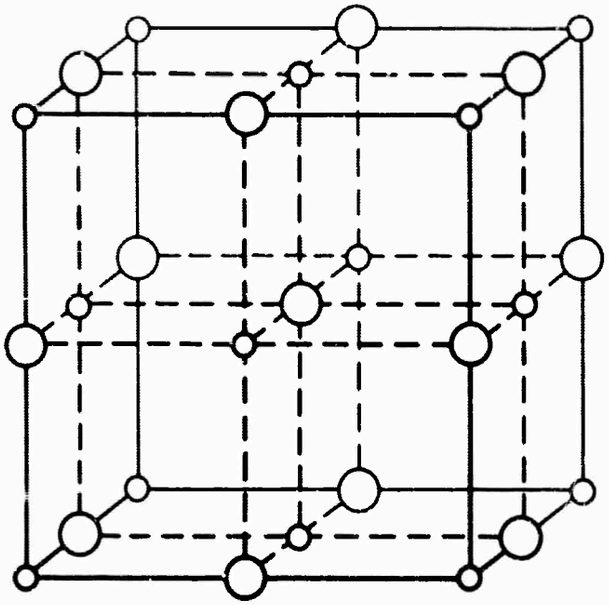

a) NaCl STRUCTURE

○ = Na ◯ = Cl

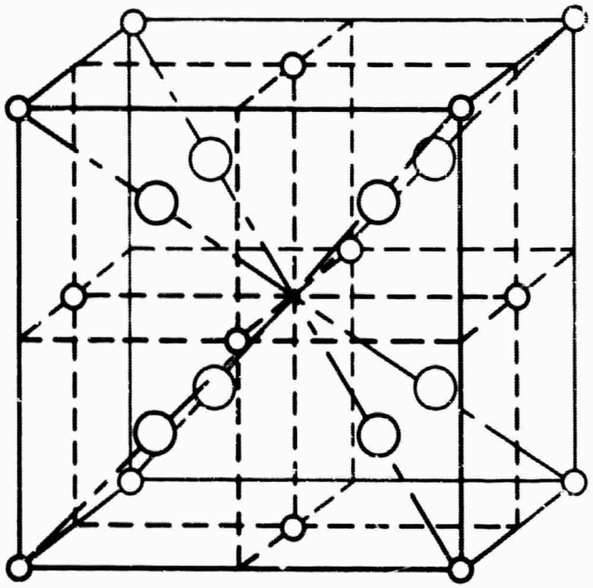

b) CaF_2 STRUCTURE

○ = Ca ◯ = F

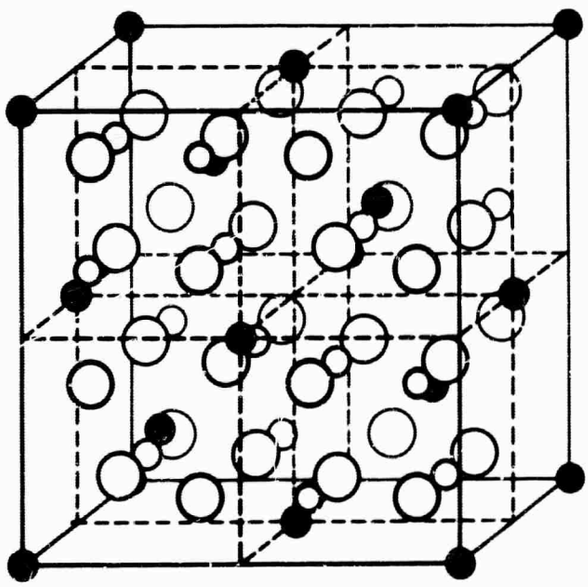

c) SPINEL STRUCTURE

AB_2O_4

● = A ○ = B ◯ = O

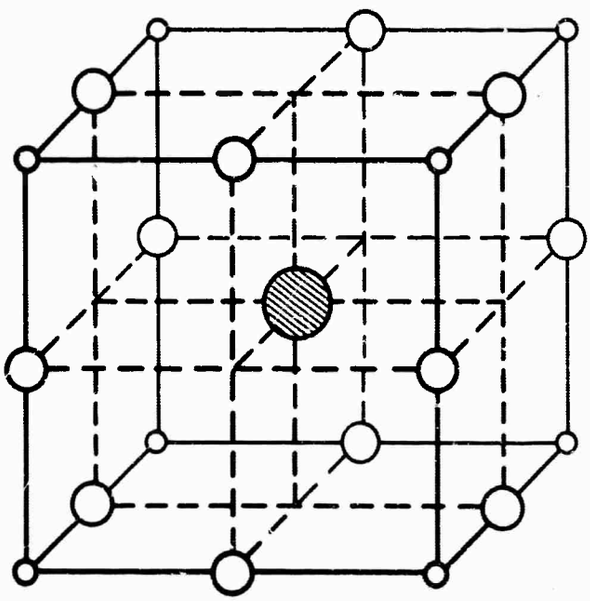

d) PEROVSKITE STRUCTURE

ABO_3

▨ = A ○ = B ◯ = O

ORDERED PEROVSKITE STRUCTURES

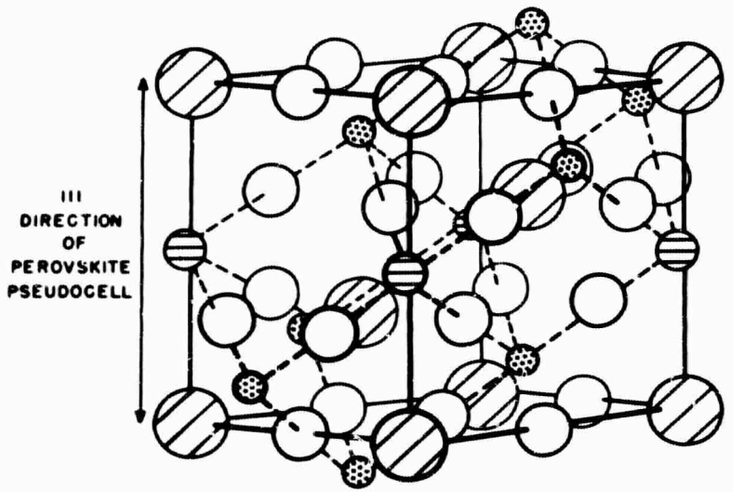

a) HEXAGONAL ORDERED PEROVSKITE-TYPE $Ba(B'_{0.33}B''_{0.67})O_3$

= A, = B', = B'', = O

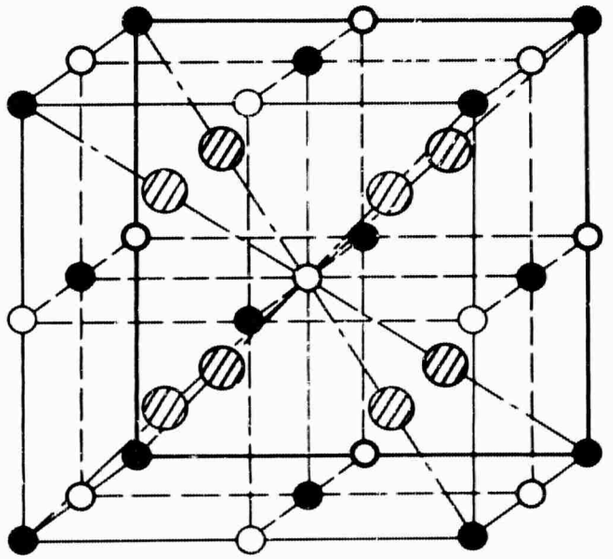

b) CATION POSITIONS IN CUBIC ORDERED PEROVSKITE-TYPE $Ba(B'_{0.5}B''_{0.5})O_3$

= A, = B', = B''

(OXYGEN ANION POSITIONS ARE CENTERED ON THE LINES BETWEEN THE B' AND B'' CATIONS)

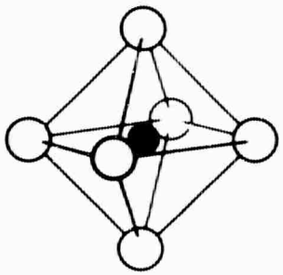

OXYGEN OCTAHEDRON AROUND B CATION

ORDERED NaCl STRUCTURES

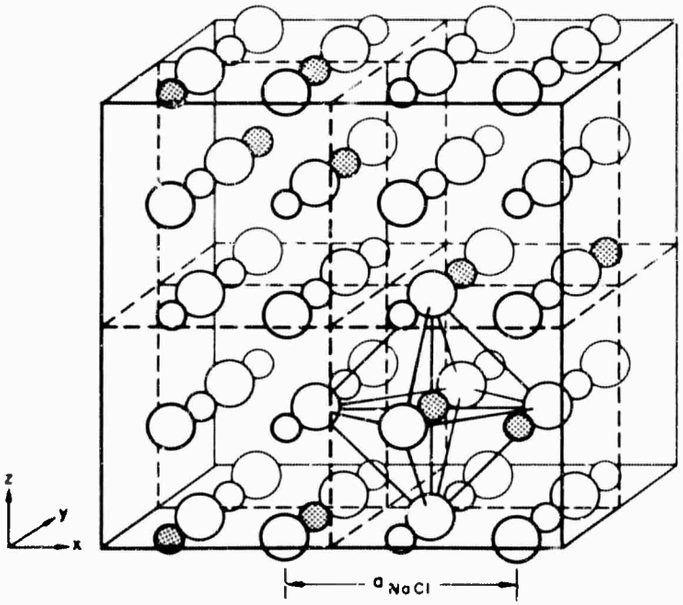

a) CUBIC, Li_3NbO_4

○ = Li ◉ = Nb ◯ = O

CATION POSITIONS AT ONE-QUARTER LEVELS IN UNIT CELL

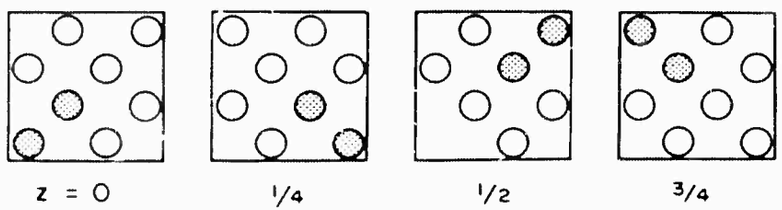

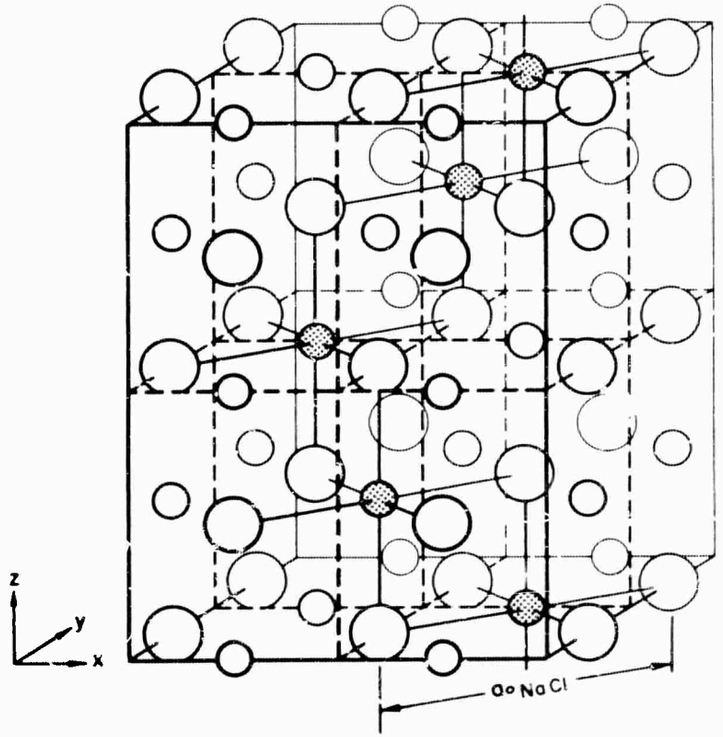

b) TETRAGONAL DISTORTION, Li_3SbO_4

○ = Li ◉ = Sb ◯ = O

CATION POSITIONS AT ONE-QUARTER LEVELS IN UNIT CELL

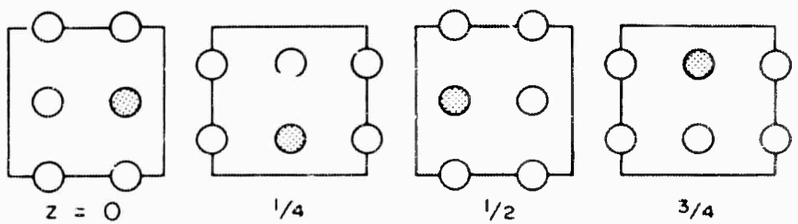

FIG. 3

FIG. 4

ORDERED SPINEL STRUCTURE, $ZnLiNbO_4$

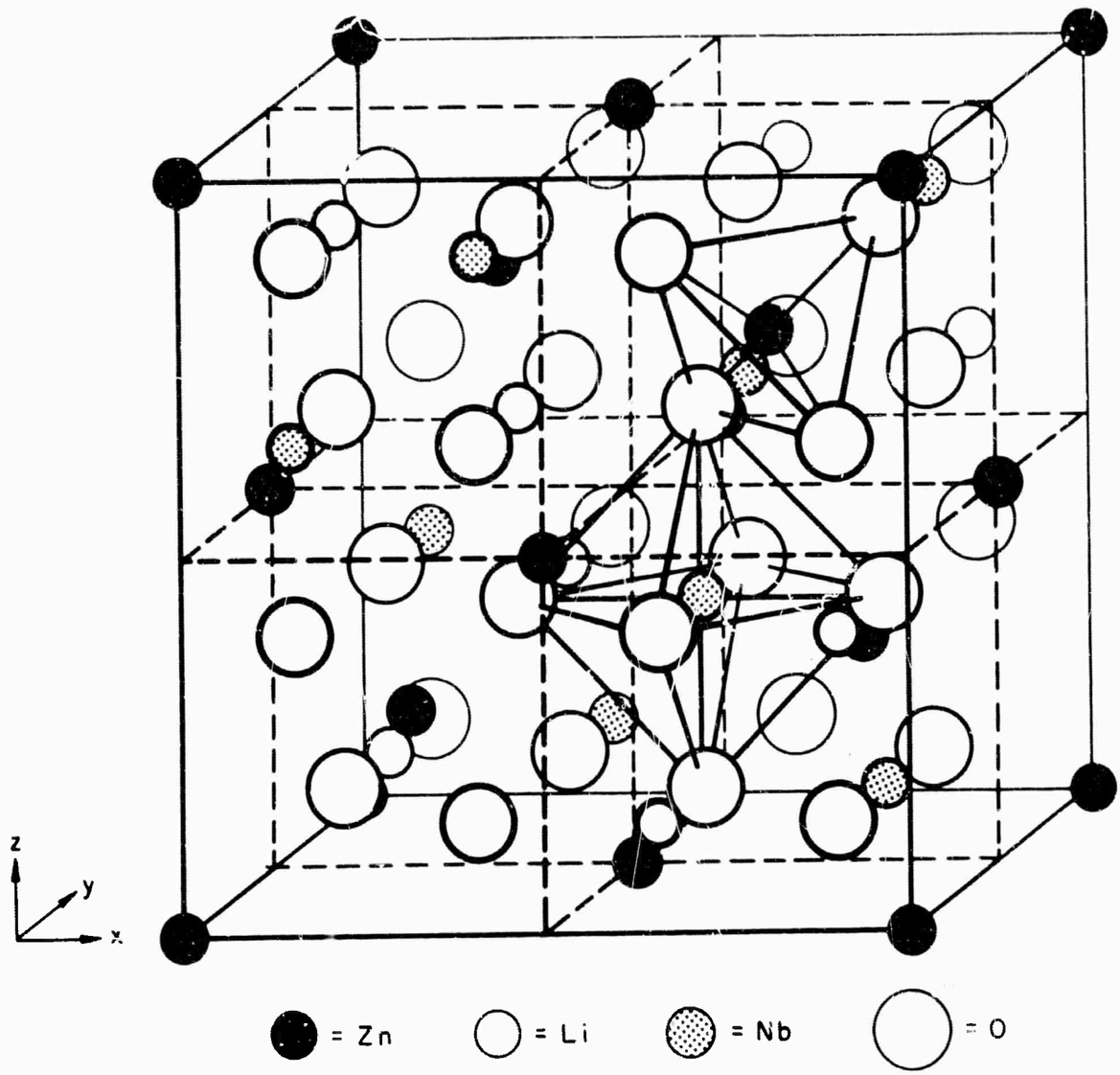

CATION POSITIONS AT ONE-EIGHTH LEVELS IN UNIT CELL

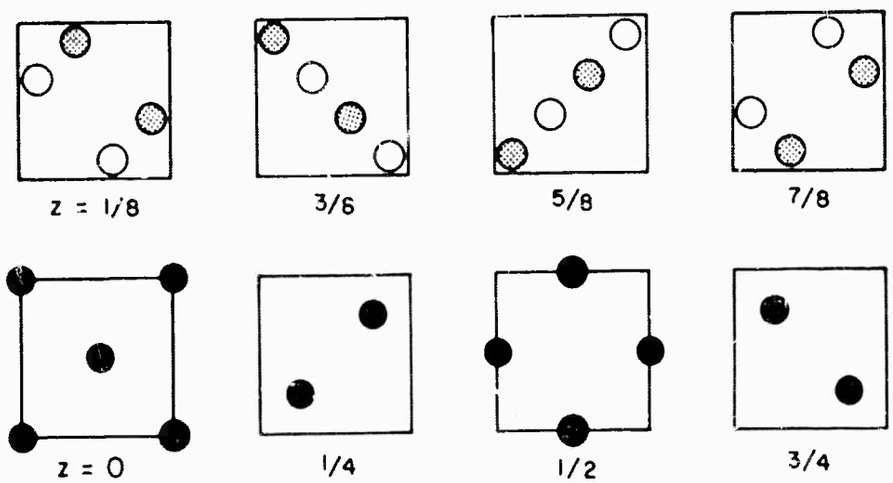

FIG. 5

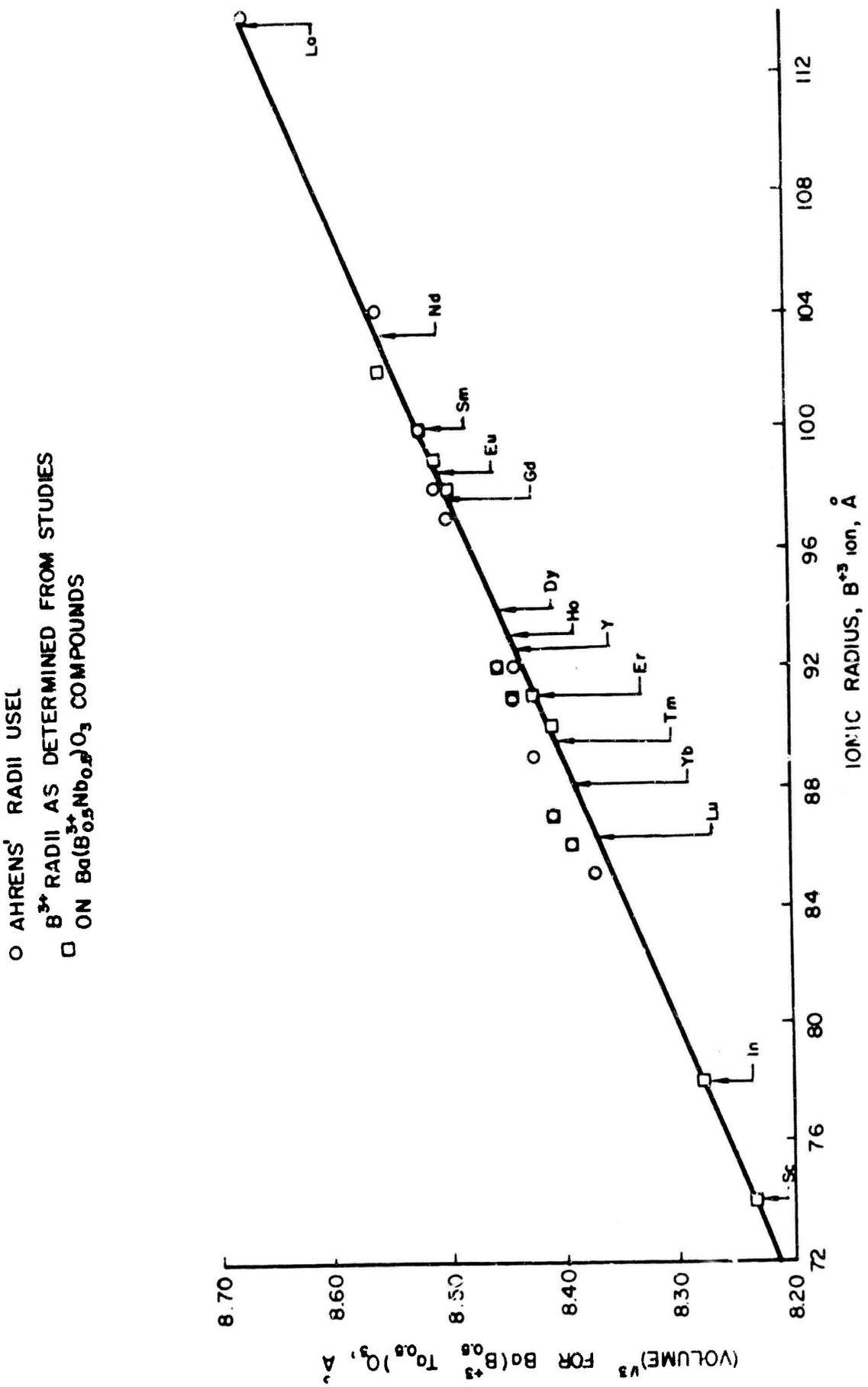
(CELL VOLUME)^1/3 VS. IONIC RADII FOR Ba(B^3+_0.5 Ta_0.5)O_3 COMPOUNDS
○ AHRENS' RADII USEL
□ B^3+ RADII AS DETERMINED FROM STUDIES ON Ba(B^3+_0.5Nb_0.5)O_3 COMPOUNDS
(VOLUME)^1/3 FOR Ba(B^+3_0.5 Ta_0.5)O_3, Å
IONIC RADIUS, B^+3 ion, Å
8.70
8.60
8.50
8.40
8.30
8.20
72
76
80
84
88
92
96
100
104
108
112
La
Nd
Sm
Eu
Gd
Dy
Ho
Y
Er
Tm
Yb
Lu
In
Sc

D910269-3

FIG. 6

$BaY_{0.5}Ta_{0.5}O_3$ CRYSTALS

GROWN FROM BaF_2 FLUX (85 w%)
BY COOLING FROM 1400°C AT 12°C/hr.
MAGNIFICATION: 10 X

D910269-3

FIG. 7

SOLUBILITY OF $Ba(Y_{0.5}Ta_{0.5})O_3$ IN BaF_2

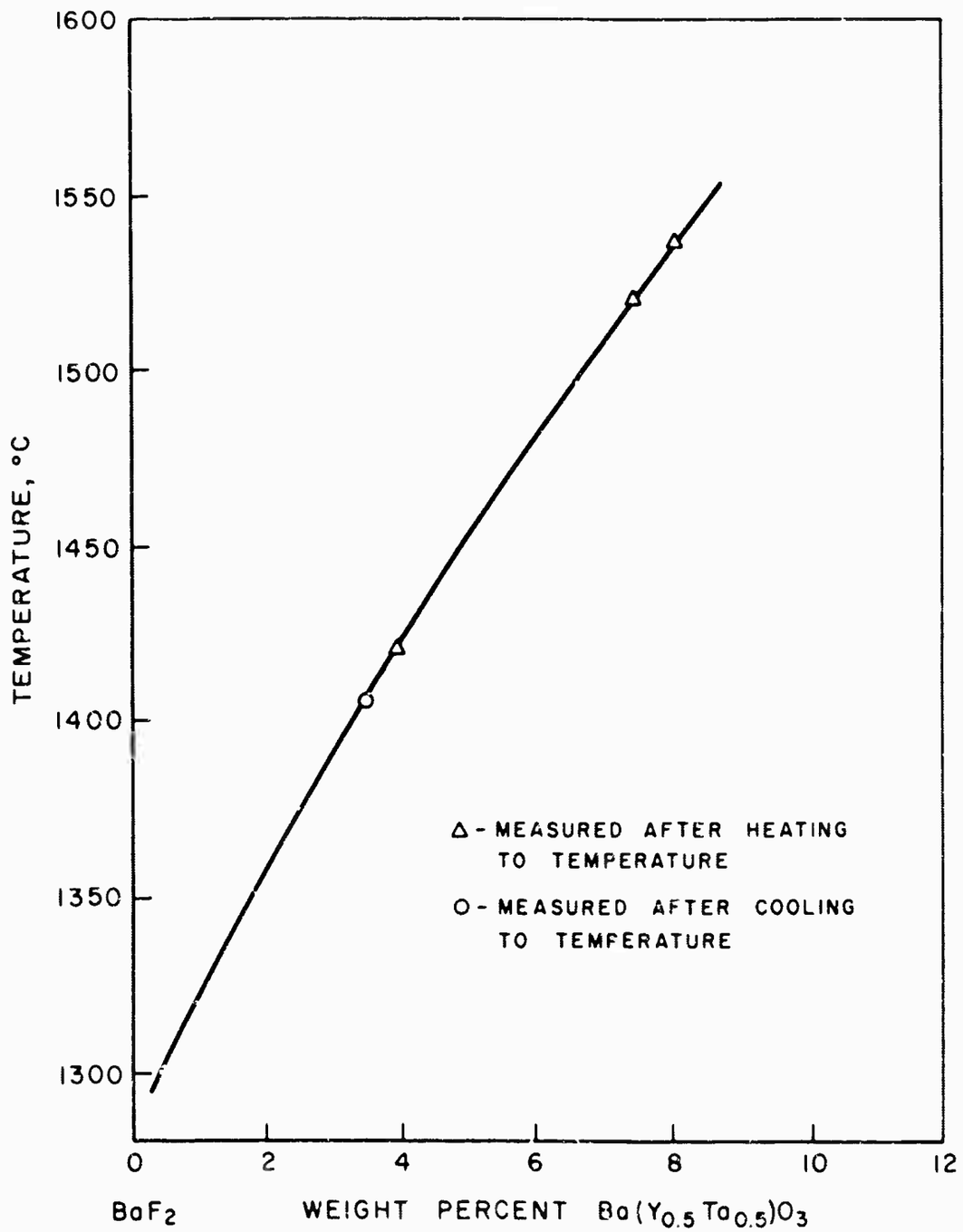

FIG. 8

BORON NITRIDE CRUCIBLE FOR GROWING CRYSTALS FROM A FLUX BY A MODIFIED BRIDGEMAN TECHNIQUE

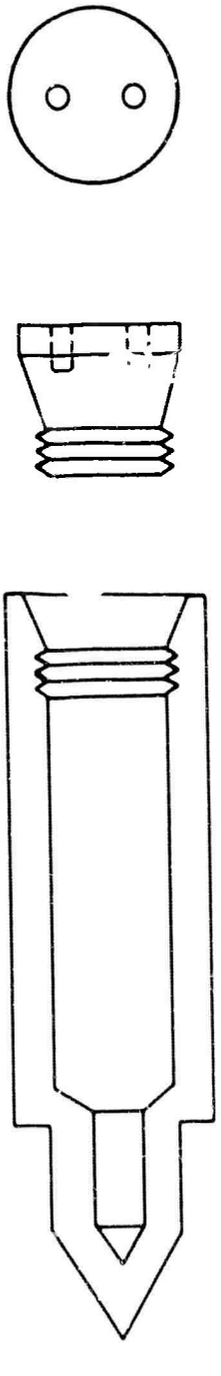

D910269-3

FIG. 9

TEMPERATURE AND CONVECTION PROFILE OF MELT IN INDUCTIVELY HEATED PLATINUM CRUCIBLE

A. OPEN CRUCIBLE
AT 1490 °C

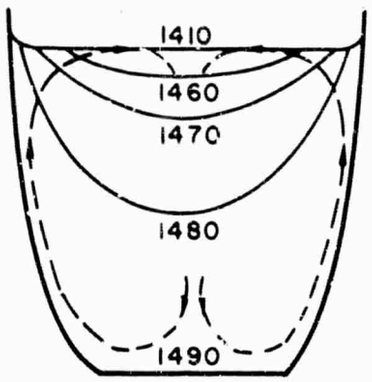

B. OPEN CRUCIBLE
AT 1445 °C

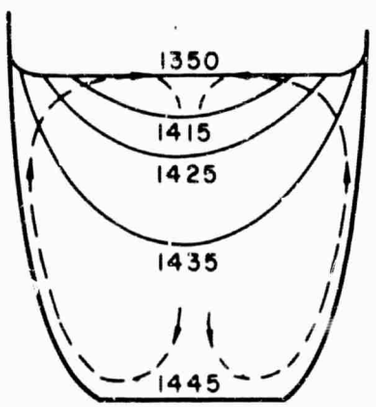

C. COVERED CRUCIBLE
AT 1440 °C

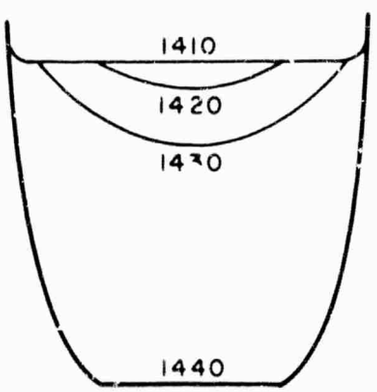

D910269-3

FIG. 10

FLUORESCENCE EMISSION OF $Ba(Sc_{.48}Nd^{3+}_{.02}Ta_{.50})O_3$ POWDER

T = 300 °K

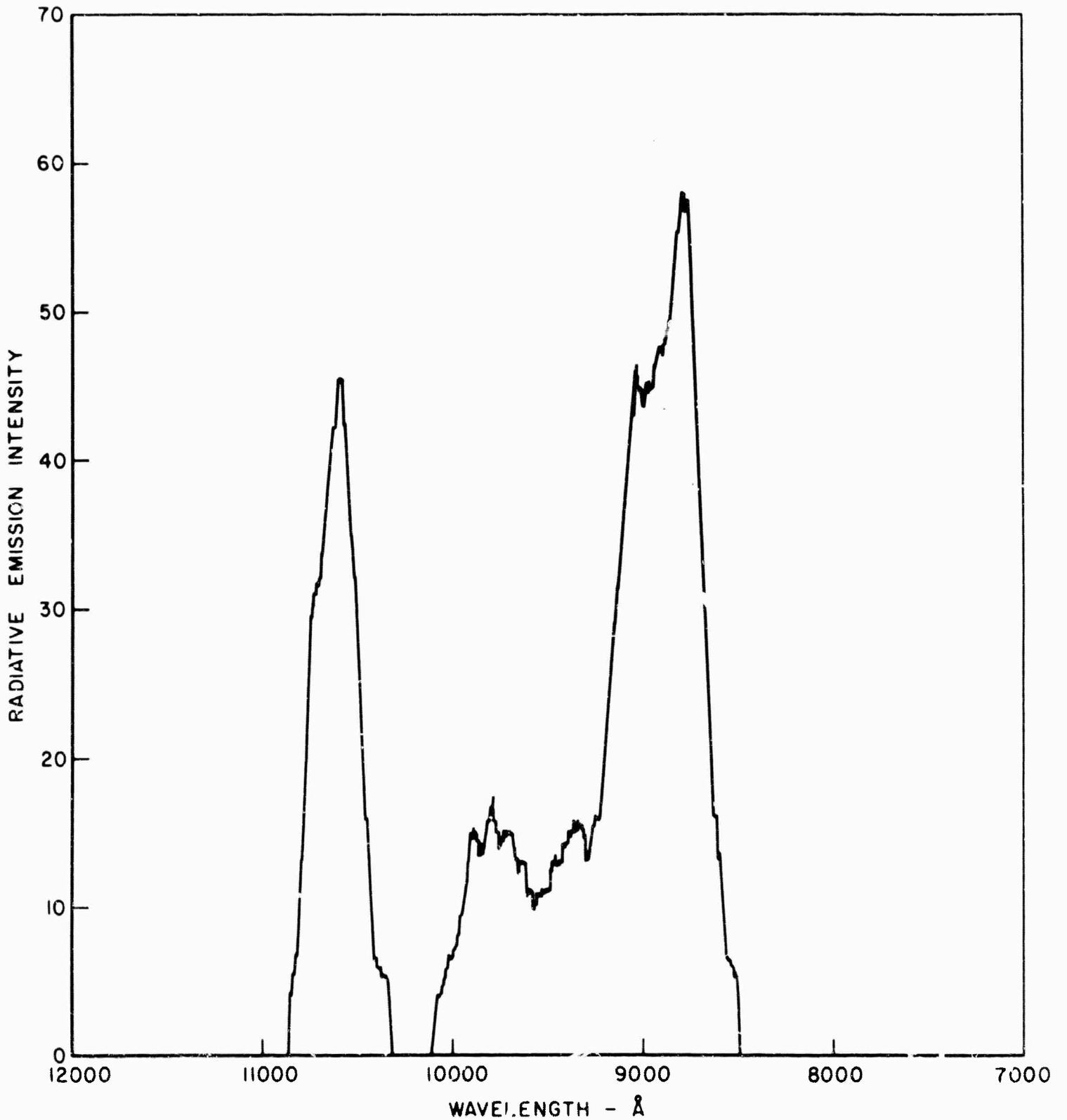

D910269-3

FIG. 11

FLUORESCENCE EMISSION OF $Ba(Sc_{.48}Nd^{3+}_{.02}Ta_{.50})O_3$ POWDER

T = 77 °K

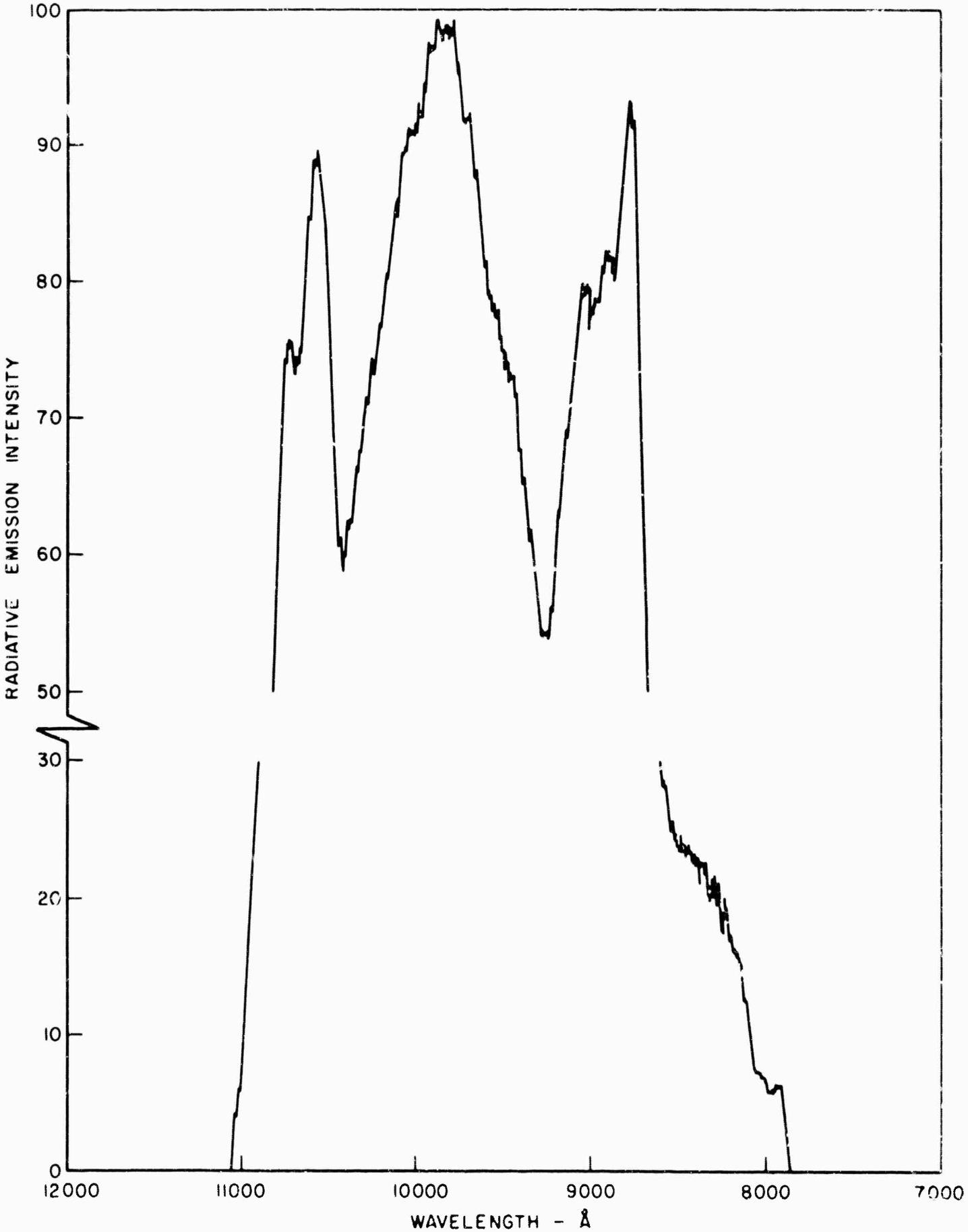

FIG. 12

FLUORESCENCE EMISSION OF $Ba(Y_{.495}Nd^{3+}_{.005}Ta_{.500})O_3$ POWDER

T = 300 °K

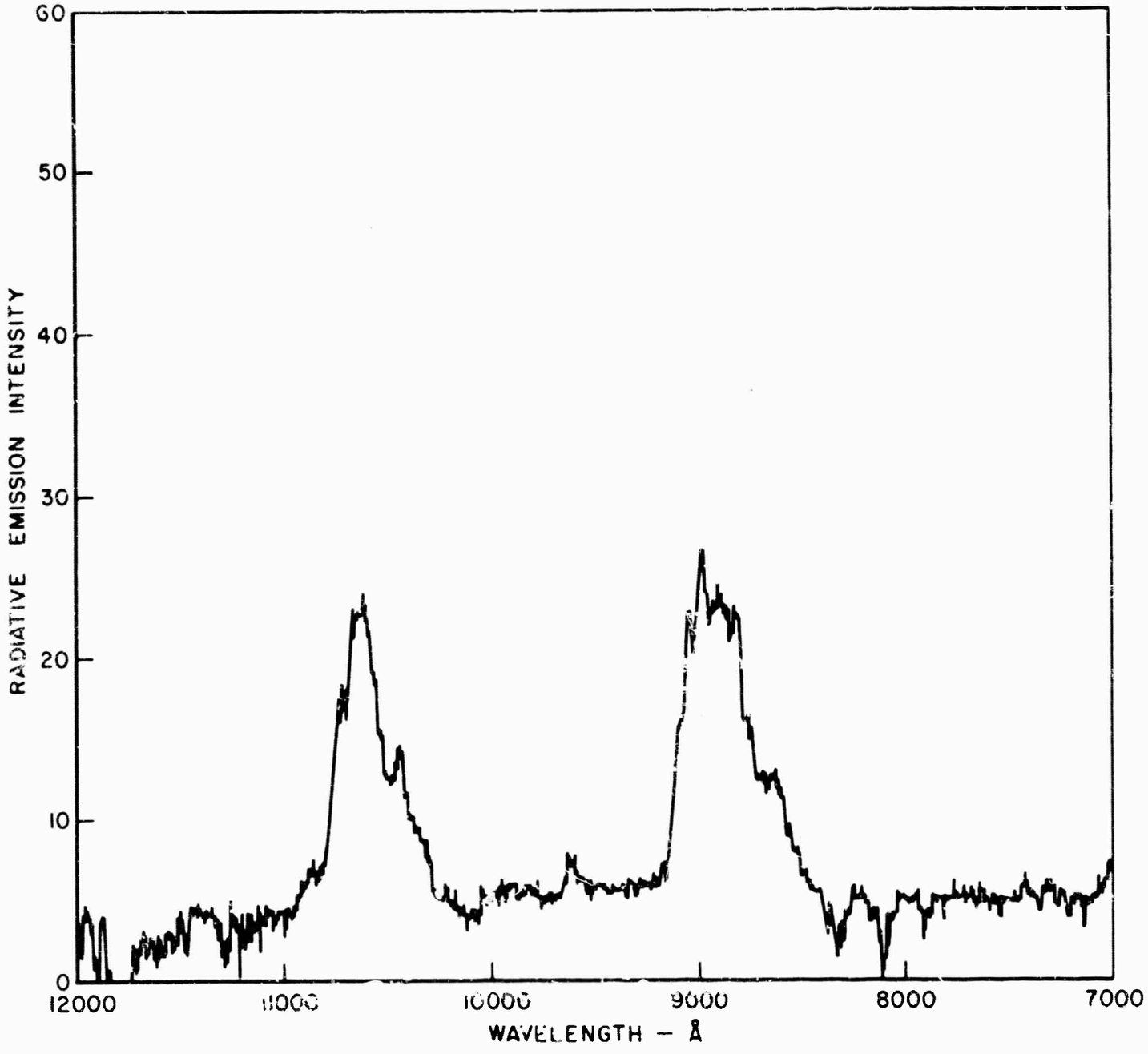

FIG. 13

FLUORESCENCE EMISSION OF $Ba(Y_{.495}Nd^{3+}_{.005}Ta_{.50})O_3$ POWDER

T = 77 °K

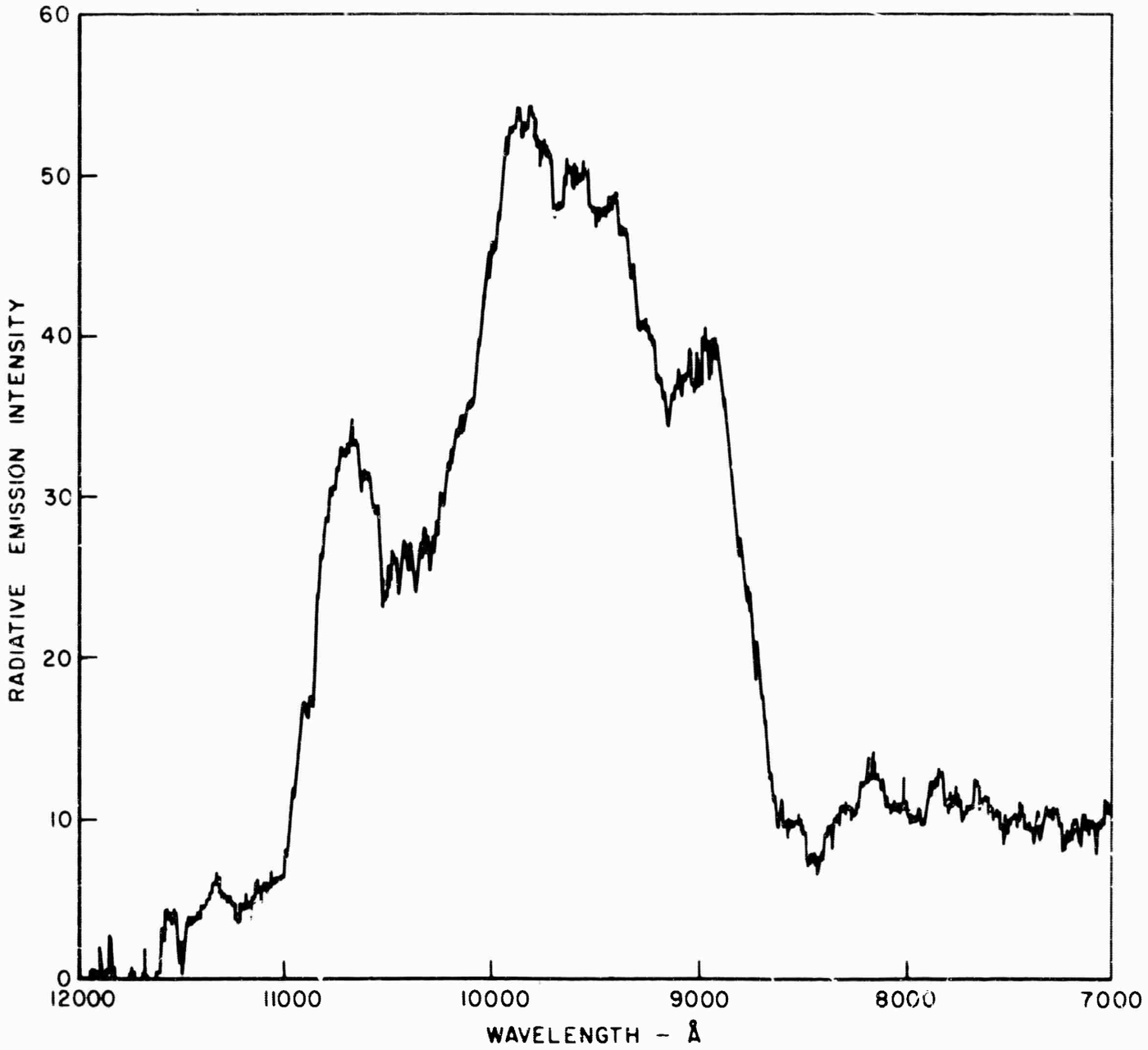

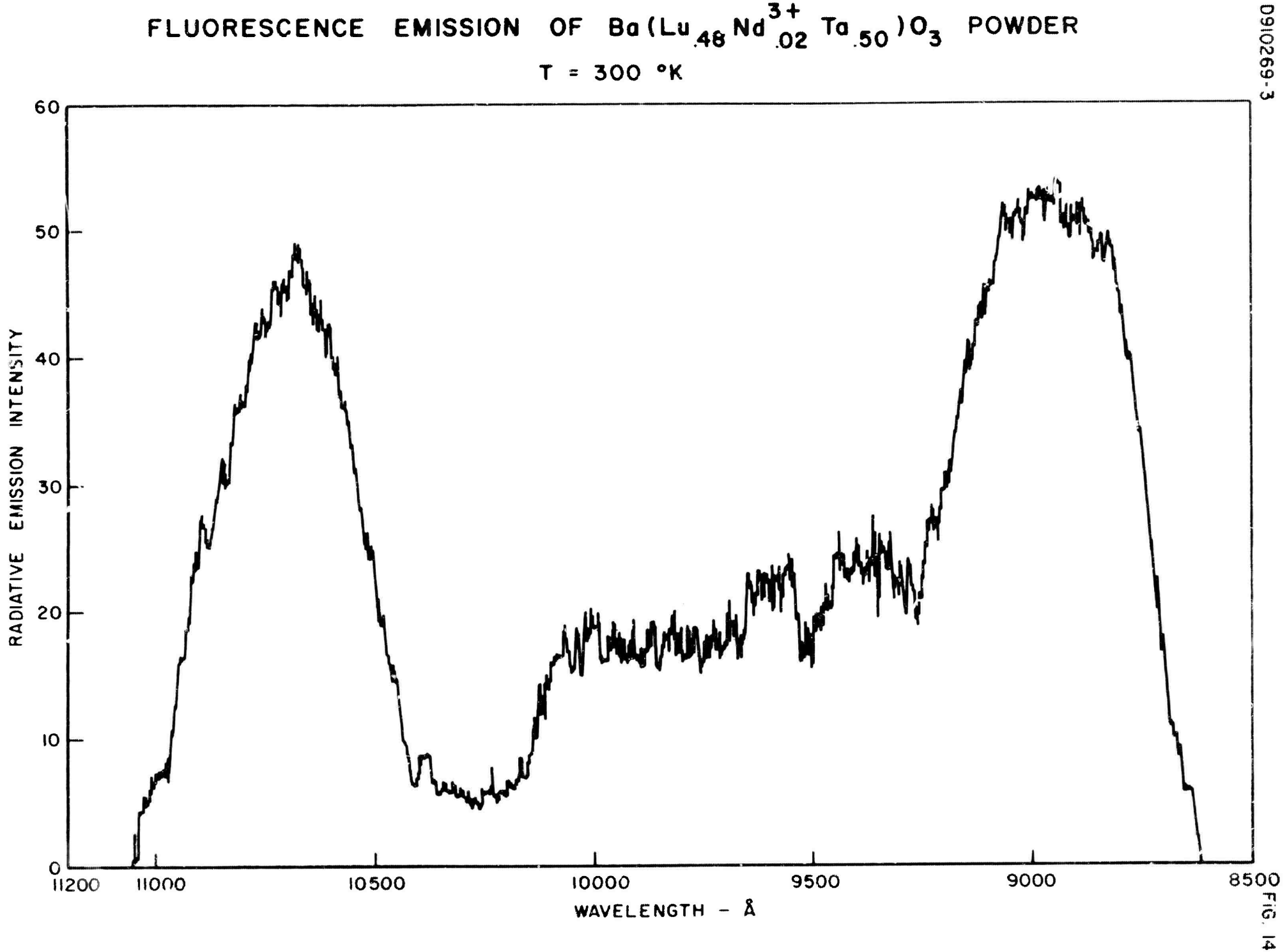
FLUORESCENCE EMISSION OF $Ba(Lu_{.48}Nd^{3+}_{.02}Ta_{.50})O_3$ POWDER
T = 300 °K
0910269-3
RADIATIVE EMISSION INTENSITY
0
10
20
30
40
50
60
11200
11000
10500
10000
9500
9000
8500
WAVELENGTH - Å

FIG. 14

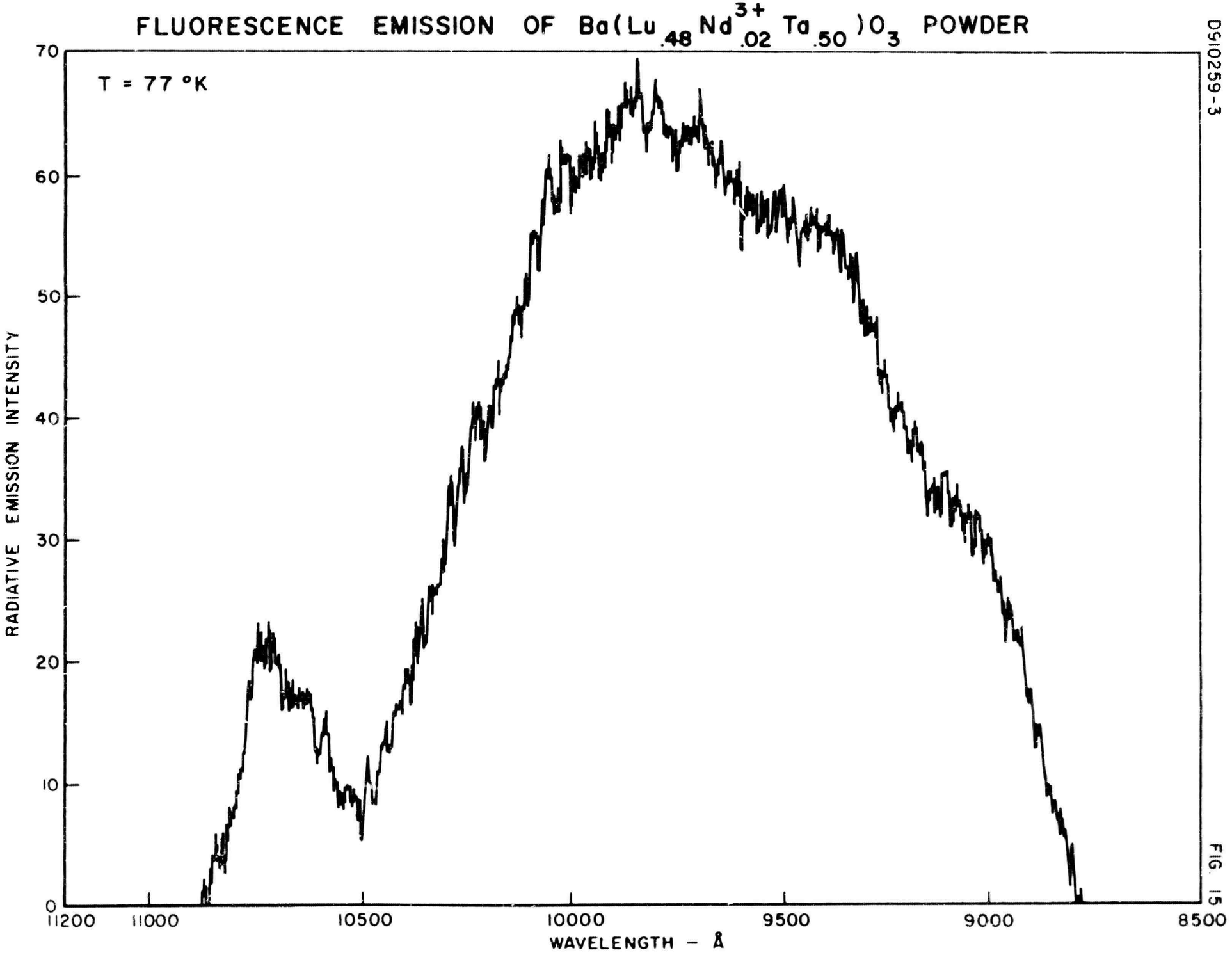
FLUORESCENCE EMISSION OF $Ba(Lu_{.48}Nd^{3+}_{.02}Ta_{.50})O_3$ POWDER
T = 77 °K
RADIATIVE EMISSION INTENSITY
0
10
20
30
40
50
60
70
11200
11000
10500
10000
9500
9000
8500
WAVELENGTH – Å
D910259-3
FIG. 15

ROTATING CRUCIBLE HOLDER

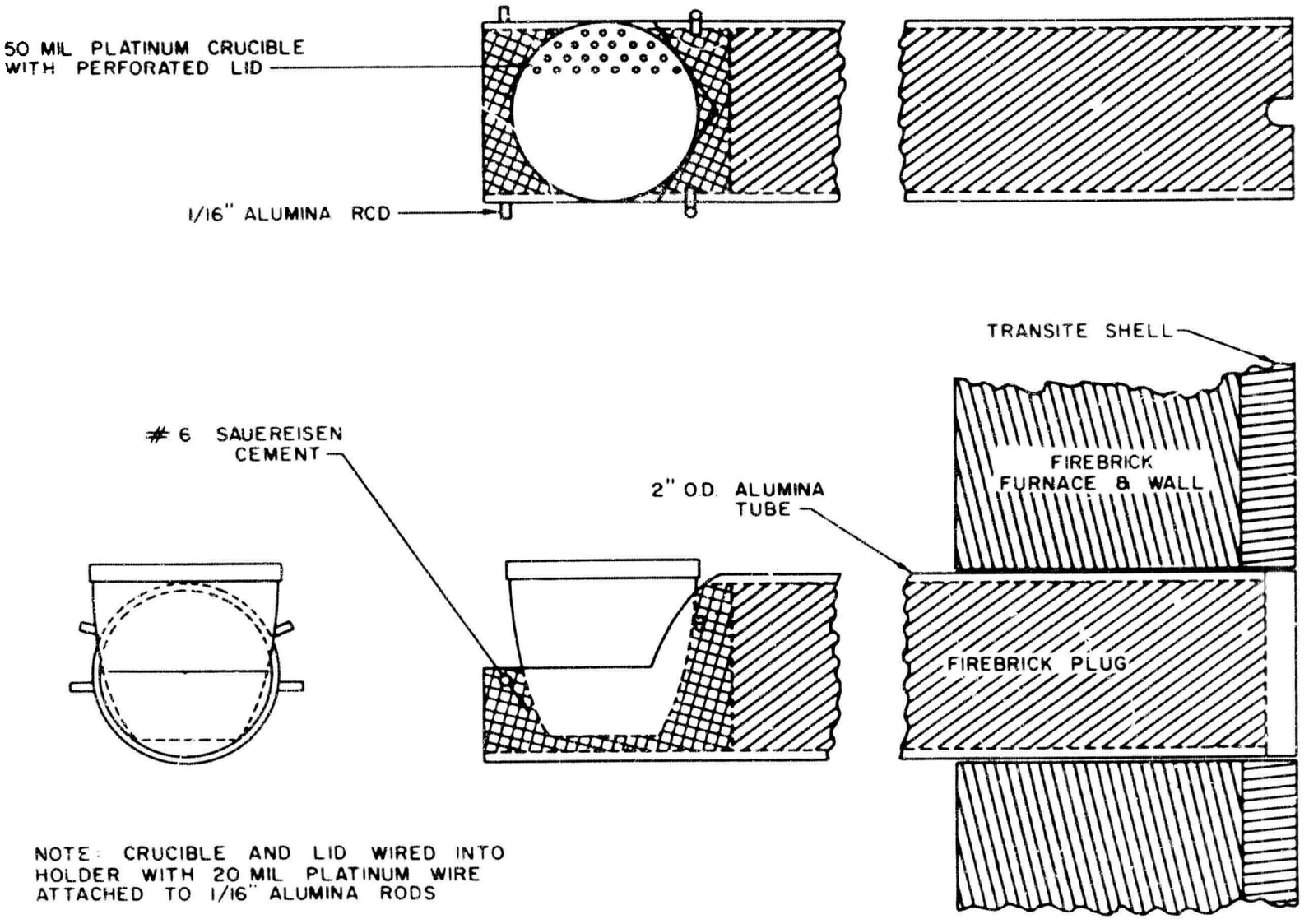

NOTE: CRUCIBLE AND LID WIRED INTO HOLDER WITH 20 MIL PLATINUM WIRE ATTACHED TO 1/16" ALUMINA RODS

D910269-3

FIG. 16

FIG. 17

GRADIENT FURNACE

SCALE 1 cm = 1 inch

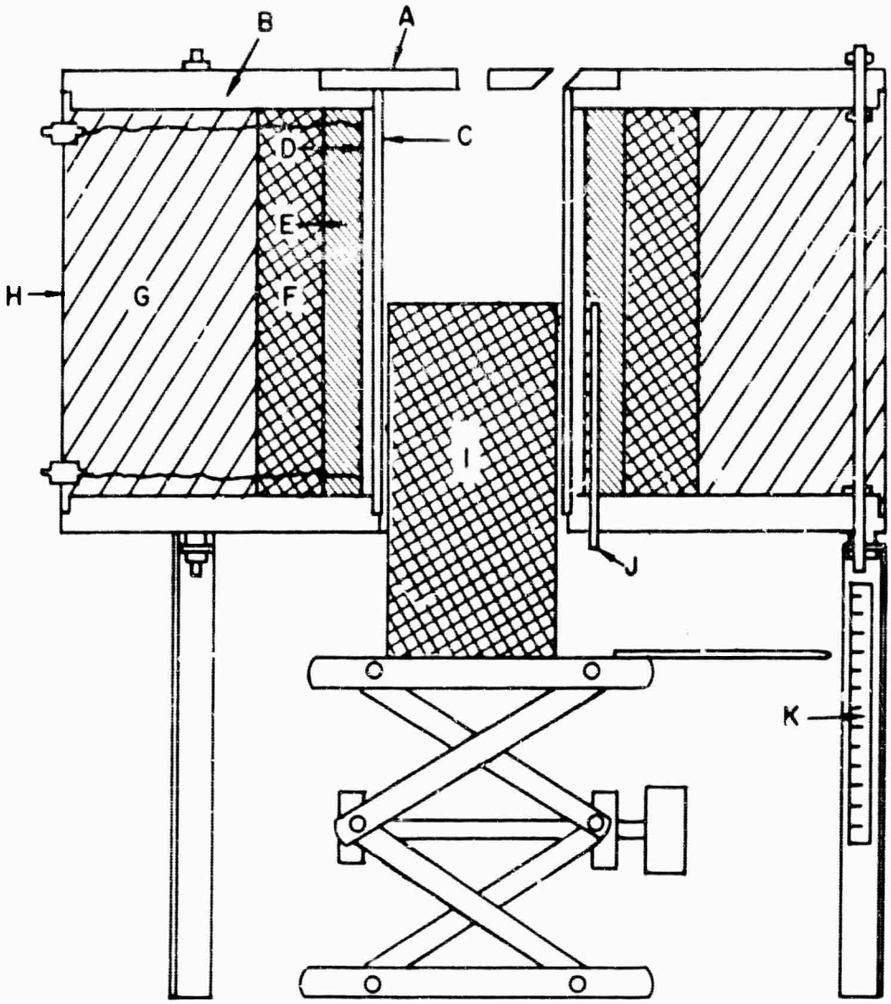

A) ZIRCONIA COVER

B) TRANSITE- top and bottom

C) 1/8" WALL ALUMINA MUFFLE

D) .032" pt/40 rh WINDING - 10 turns per inch

E) CASTABLE ALUMINA AND ALUMINA BUBBLES

F) K-30 FIREBRICK

G) CERAFELT ●

H) ALUMINA SHELL

I) K-30 FIREBRICK PLUG

J) CONTROL THERMOCOUPLE

K) POSITIONING SCALE

FIG. 18

SAMPLE 65-00 2e, 57 w/o BaO, 28 w/o $YTaO_4$, 15 w/o B_2O_3

QUENCHED FROM 1480 °C
IMMERSED IN OIL OF INDEX 1.75
MAGNIFICATION: 200 X

GLASS HAS PARTIALLY DEVITRIFIED, RESULTING IN THE INCLUSION OF VERY SMALL QUENCHING CRYSTALS

D910269-3

FIG. 19

SAMPLE 64-427 f, 41.8 w/o BaO, 45.7 w/o $YTaO_4$, 12.5 w/o B_2O_3

QUENCHED FROM 1432 °C
IMMERSED IN OIL OF INDEX 1.75
MAGNIFICATION: 200 X

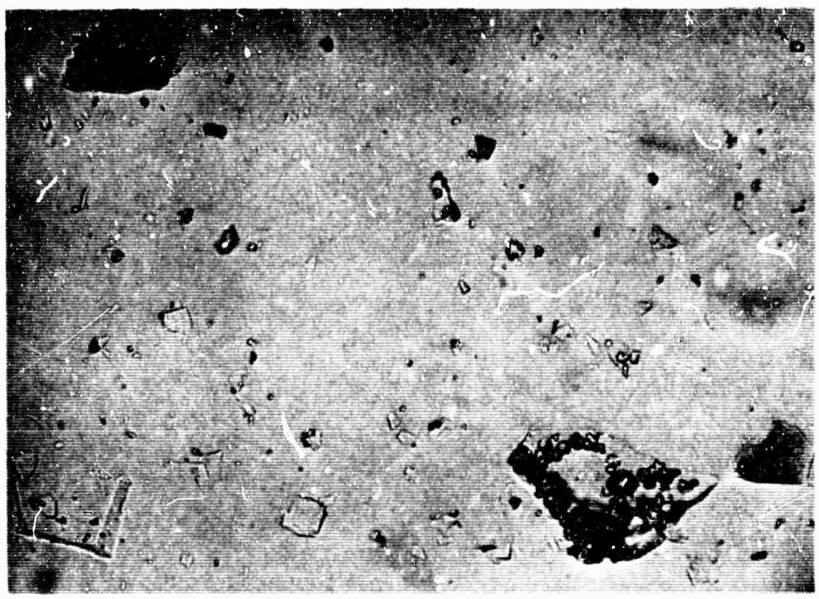

CHIPS OF CLEAN GLASS MAY BE SEEN, AS WELL AS GLASS CONTAINING QUENCHING CRYSTALS, AND GLASS CONTAINING PRIMARY CRYSTALS

FIG 20

PORTION OF THE JOIN
$BaY_{0.5}Ta_{0.5}O_3$ - B_2O_3

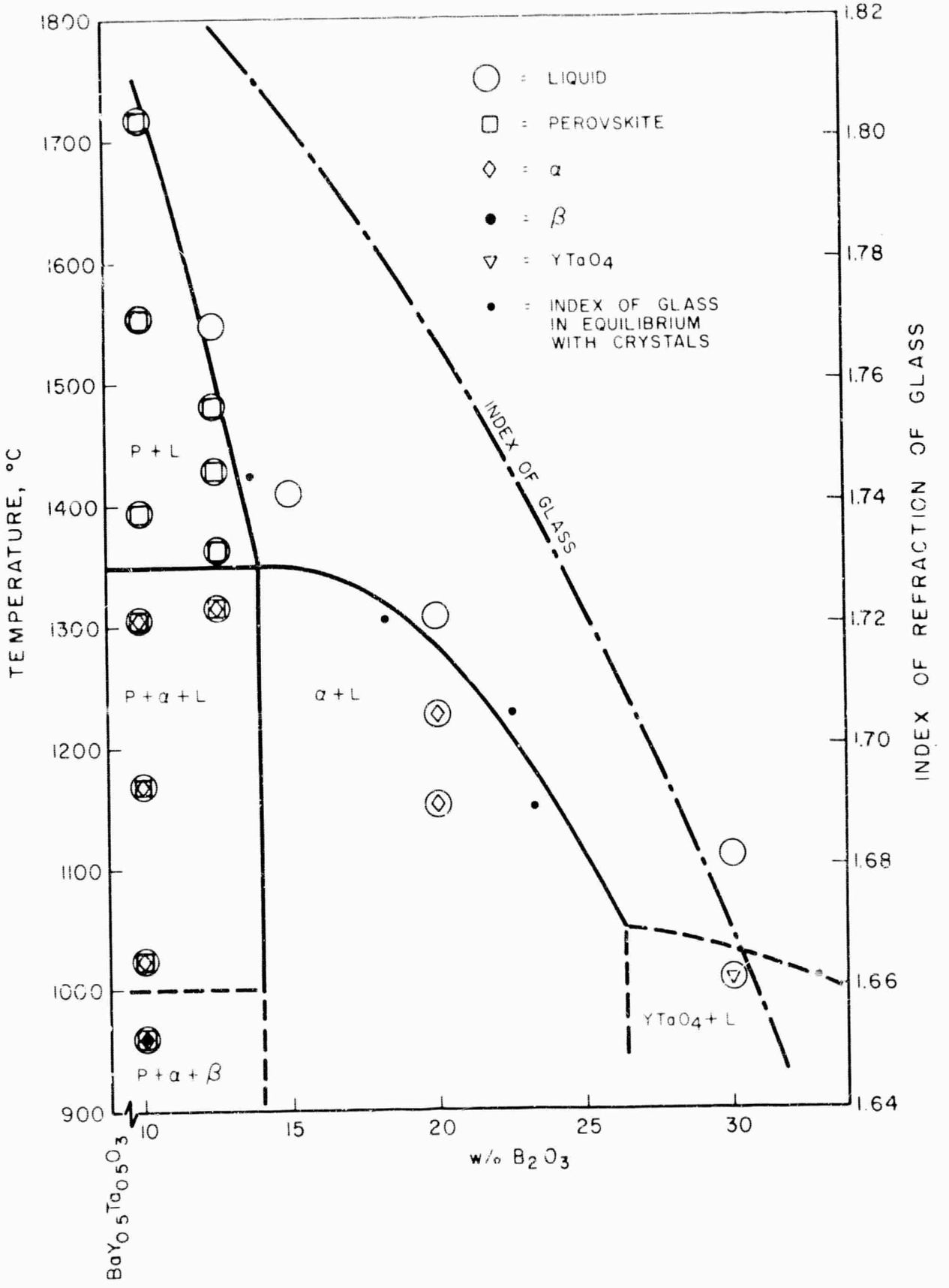

D910269-3

FIG. 21

PORTION OF THE JOIN $BaY_{0.5}Ta_{0.5}O_3$ - BaB_8O_{13}

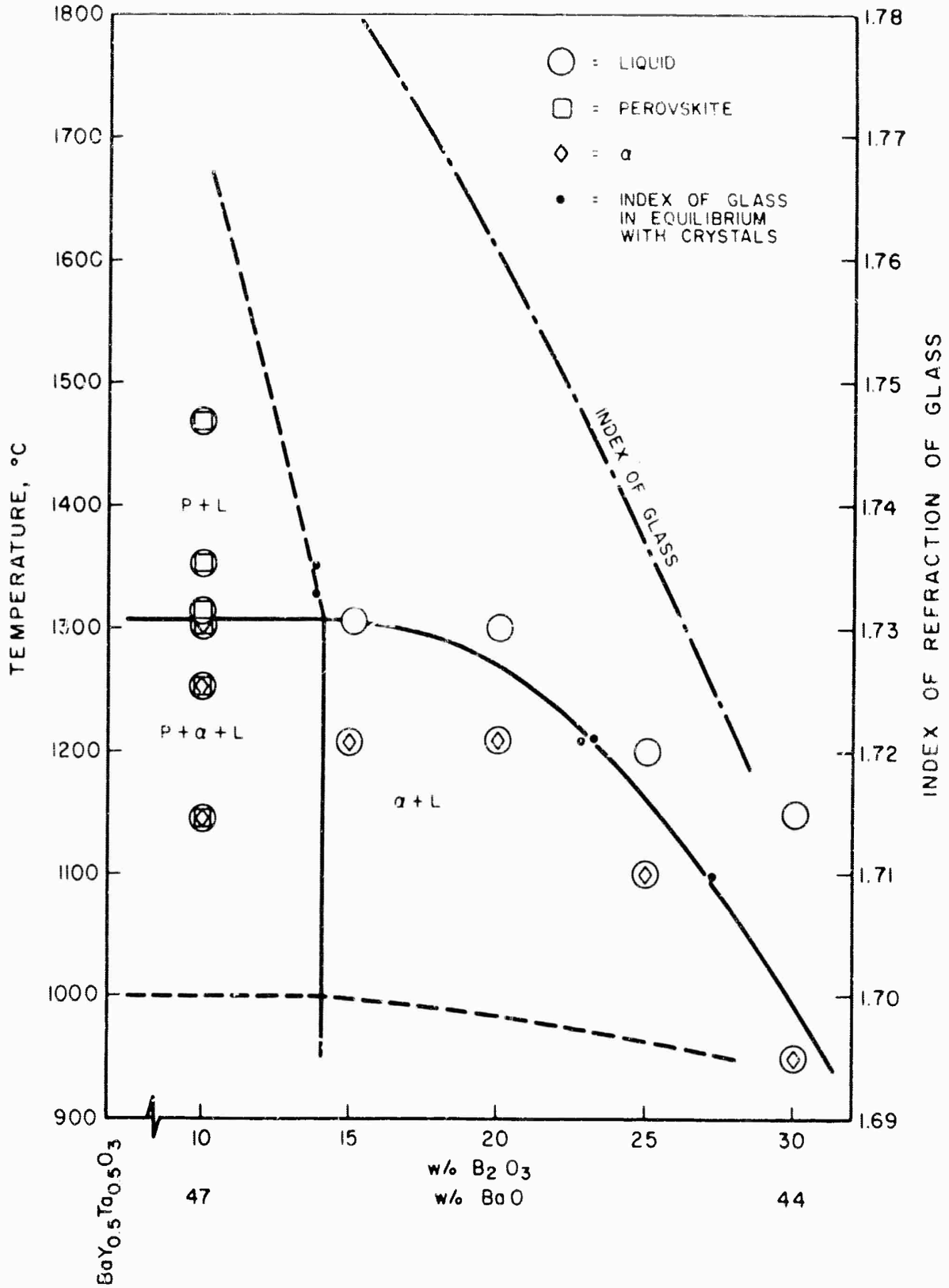

FIG 22

PORTION OF THE JOIN
$BaY_{0.5}Ta_{0.5}O_3$ - BaB_2O_4

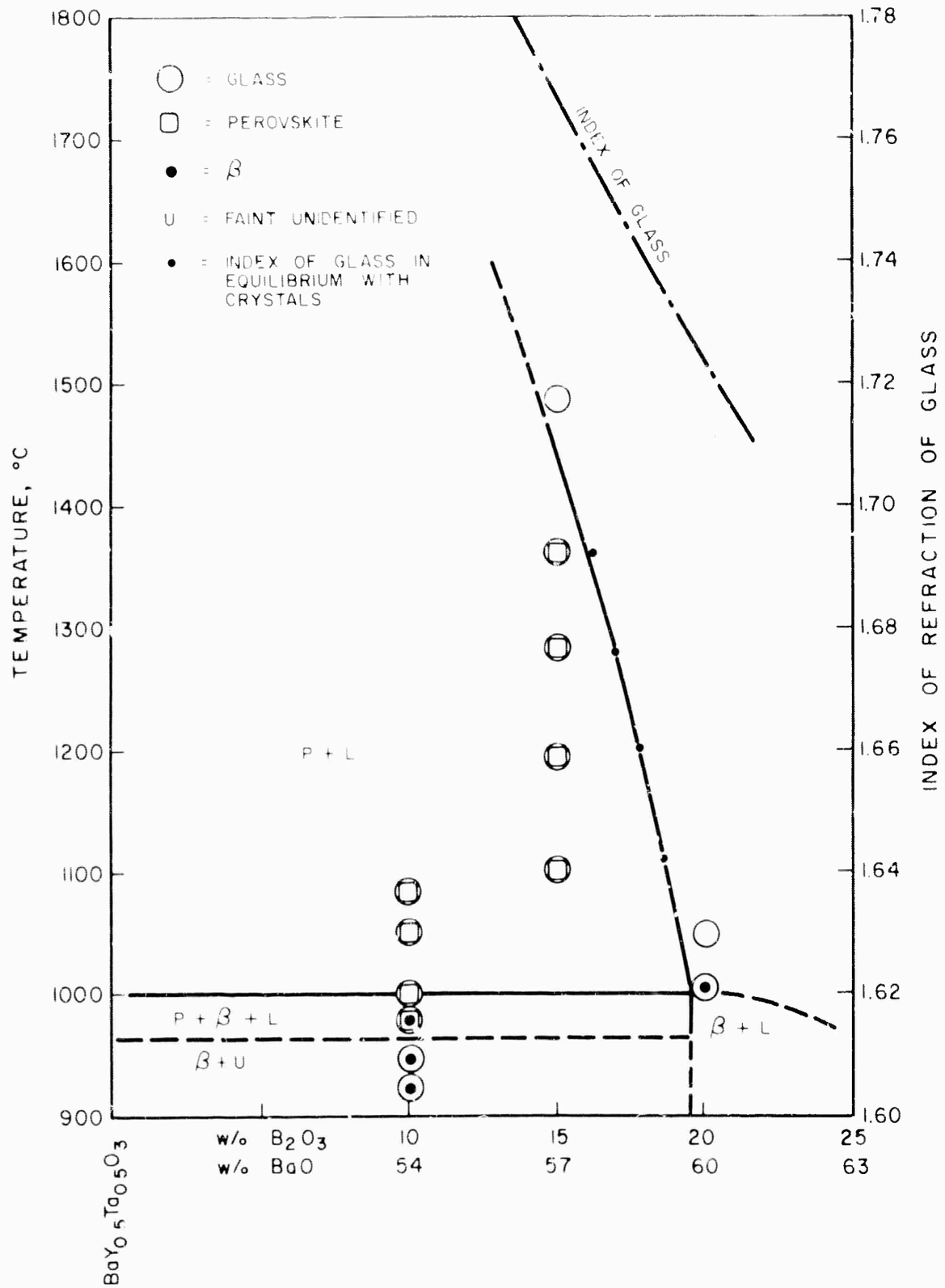

D910269-3

FIG 23

PRIMARY PHASE REGIONS AROUND THE PEROVSKITE FIELD IN THE PSUEDO-TERNARY SYSTEM BaO-$YTaO_4$-B_2O_3

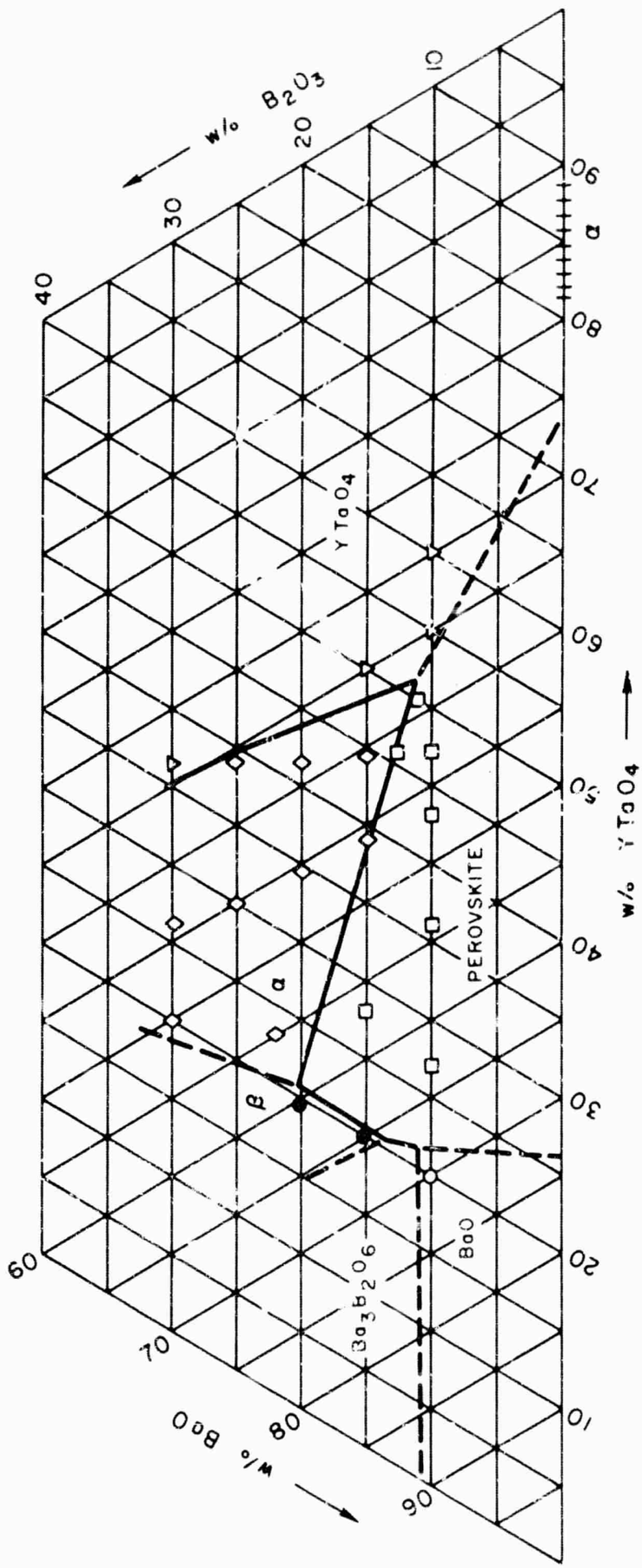

FIG. 24

PSUEDO-TERNARY SYSTEM BaO-YTaO4-B2O3

(PARTIAL DIAGRAM OF LIQUIDUS SURFACE)

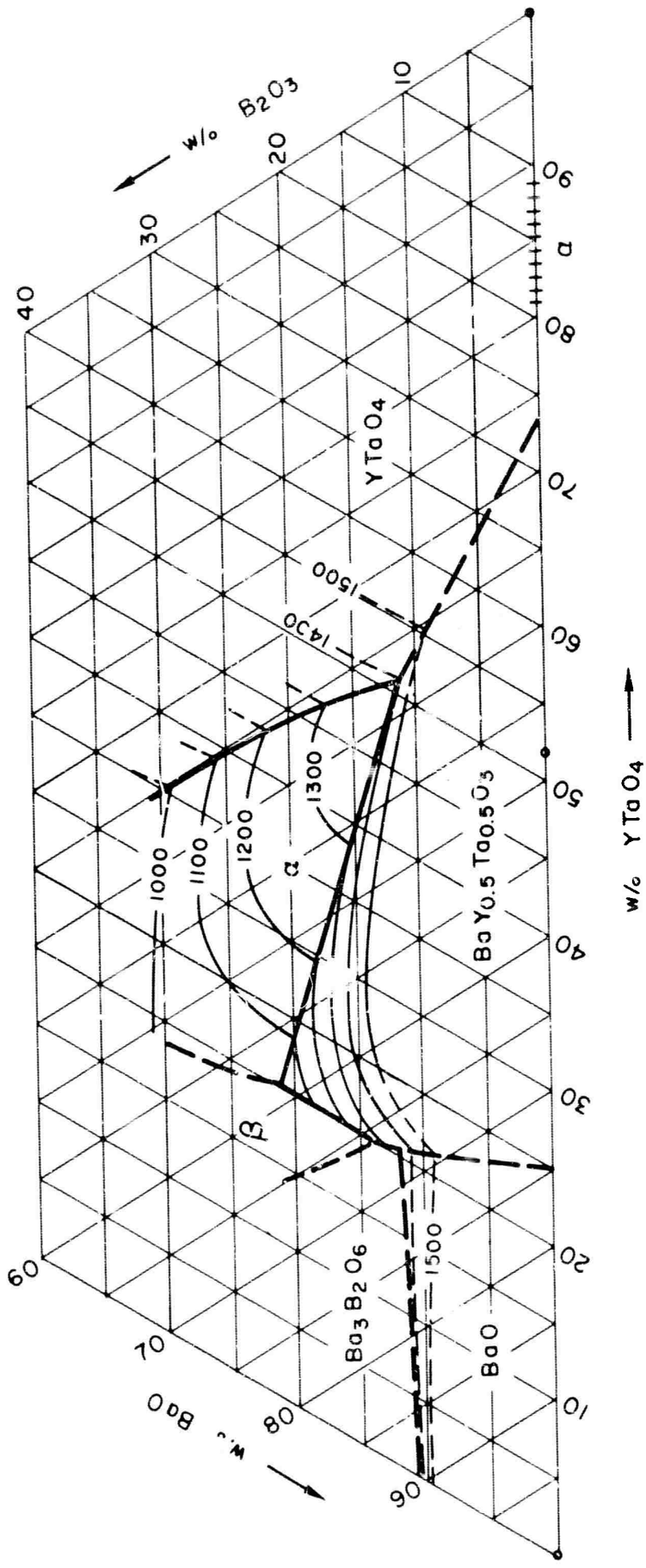

FIG. 25

LOG RESISTIVITY VS 1000/T FOR $La(Ni_{0.5}Ru_{0.5})O_3$ AND $La(Mg_{0.5}Ru_{0.5})O_3$

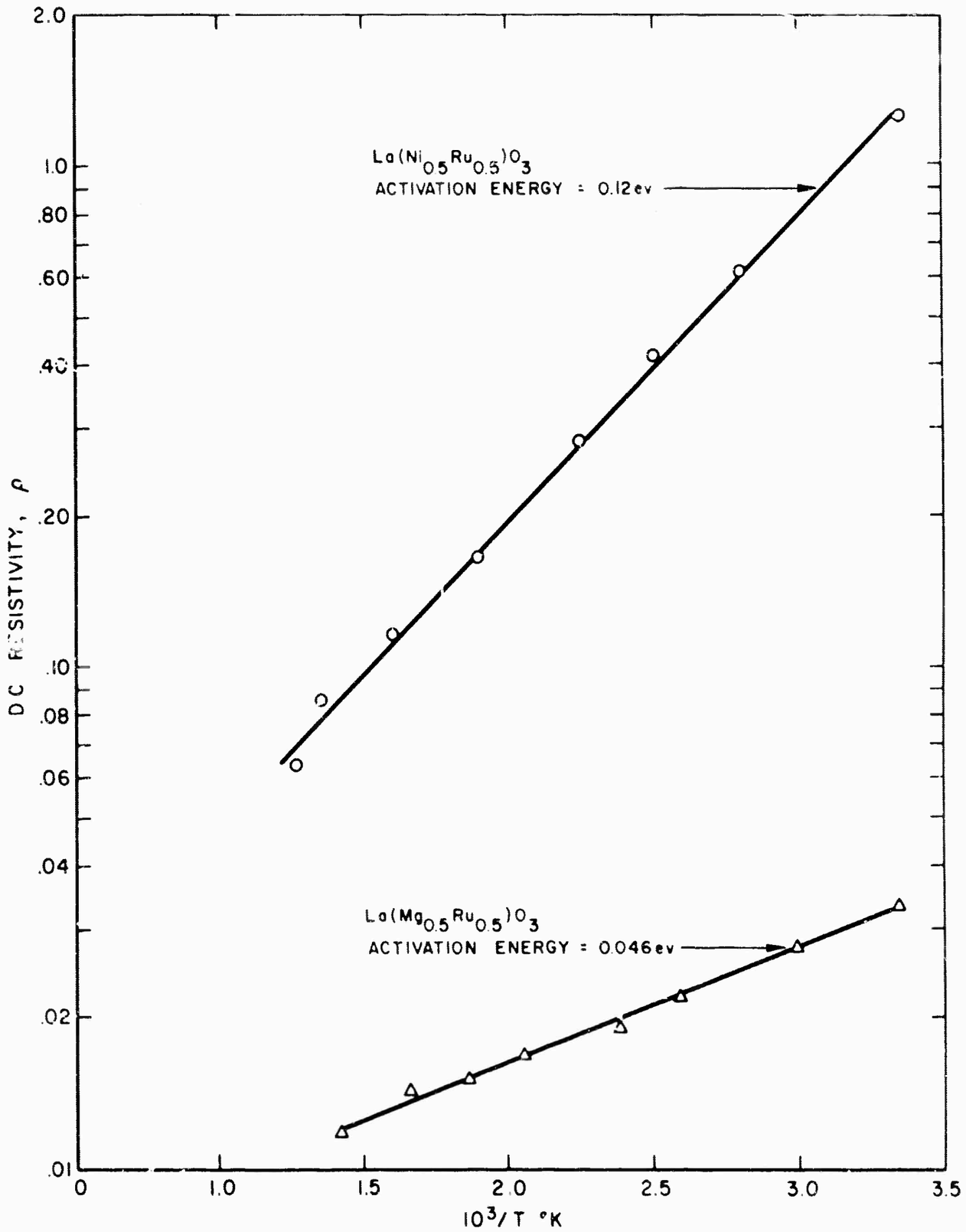

DISTRIBUTION LIST FOR UNITED AIRCRAFT CORPORATION

Contract No. Nonr-4606(00)

Semiannual Report

	No. of Copies
R. S. Congleton Hughes Aircraft Corp. Aerospace Group Research & Development Division Culver City, California	1
Basil Curnutte, Jr. Kansas State University Manhattan, Kansas	1
G. H. Dieke Johns Hopkins University Baltimore 18, Maryland	1
C. H. Keller Pek Labs, Inc. 925 Evelyn Avenue Sunnyvale, California	1
S. P. Keller International Business Machines T. J. Watson Research Center Yorktown Heights, New York	1
A. Lempicki General Telephone & Electronics Labs Bayside 60, New York	1
R. C. Pastor Korad Corporation 2520 Colorado Avenue Santa Monica, California	1

T. C. McAvoy
Corning Glass Works
Corning, New York
1

W. McKusick
Eastman Kodak Company
Apparatus and Optical Division
400 Plymouth Avenue, N.
Rochester 4, New York
1

O. H. Nestor
Linde Company
1500 Polco Street
Indianapolis 24, Indiana
1

J. W. Nielson
Airtron, A Division of Litton Industries
200 East Hanover Avenue
Morris Plains, New Jersey
1

Gerald Oster
Chemistry Department
Polytechnic Institute of Brooklyn
333 Jay Street
Brooklyn 1, New York
1

David Stockman
Electronics Laboratory
General Electric Company
Syracuse, New York
1

J. W. Turner
Westinghouse Electric Corp.
Electronics Division
P. O. Box 1897
Baltimore 3, Maryland
1

R. W. Young
American Optical Company
Southbridge, Massachusetts
1

Dr. Jerald R. Izatt 1
New Mexico State University
University Park, New Mexico

Professor A. K. Kamal 1
Purdue University
School of Electrical Engineering
Lafayette, Indiana

Mr. Thomas C. Marshall 1
Columbia University
Dept. of Electrical Engineering
New York 27, New York

Mr. Charles G. Naiman 1
Mithras, Inc.
Cambridge 39, Massachusetts

Dr. J. H. Schulman 1
Solid State Division
U. S. Naval Research Laboratory
Washington 25, D. C.

Dr. Jack A. Soules 1
Physics Department
New Mexico State University
University Park, New Mexico

Dr. Arden Sher 1
Varian Associates
611 Hansen Way
Palo Alto, California

Physical Sciences Division 1
Army Research Office
Office, Chief, Research & Development
Washington 25, D. C.
Attn. Dr. Robert A. Watson

Chief Scientist 1
U. S. Army Electronics Command
Fort Monmouth, New Jersey
Attn: Dr. Hans K. Ziegler

Director, Institute for Explatory Research 1
Army Signal Research & Development Laboratory
Fort Monmouth, New Jersey
Attn: Dr. E. M. Reilley

Asst. Director of Surveillance 1
Army Signal Research & Development Laboratory
Fort Monmouth, New Jersey
Attn: Dr. Harrison J. Merrill

Director of Research & Development 1
Army Ordnance Missile Command
Huntsville, Alabama
Attn: Mr. William D. McKnight

Office, Chief of Naval Operations/OP-07T-1/ 1
Department of the Navy
Washington 25, D. C.
Attn: Mr. Ben Rosenberg

Bureau of Naval Weapons /RR-2/ 1
Department of the Navy
Washington 25, D. C.
Attn: Dr. C. H. Harry

Bureau of Ships /Code 305/ 1
Department of the Navy
Washington 25, D. C.
Attn: Dr. G. C. Sponsler

Office of Naval Research /Code 402C/ 1
Department of the Navy
Washington 25, D. C.
Attn: Dr. Sidney Reed

Office of Naval Research /Code 421/ 3
Department of the Navy
Washington 25, D. C.
Attn: Mr. Frank B. Isakson

Office of Naval Research /Code 406T/ 1
Department of the Navy
Washington 25, D. C.
Attn: Mr. J. W. Smith

Naval Research Laboratory /Code 6440/ 1
Department of the Navy
Washington 25, D. C.
Attn: Dr. C. C. Klick

Naval Research Laboratory /Code 7360/ 1
Department of the Navy
Washington 25, D. C.
Attn: Dr. L. F. Drummeter

Headquarters USAF /AFRDR-NU-3/ 1
Department of the Air Force
Washington, D. C.
Attn: Lt. Col. E. N. Myers

Research & Technology Division 1
Bolling Air Force Base
Washington, D. C.
Attn: Mr. Robert Feik

Office, Aerospace Research /MROSP/ 1
Washington 25, D. C.
Attn: Lt. Col. Ivan Atkinson

Technical Area Manager /760A/ 1
Advanced Weapons Aeronautical Systems Div.
Wright-Patterson AFB
Ohio
Attn: Mr. Don Newman

Project Engineer /5237/ 1
Aerospace Radiation Weapons
Aeronautical Systems Division
Wright-Patterson AFB
Ohio
Attn: Mr. Don Lewis

Air Force Special Weapons Center /SWRPA/ 1
Kirtland AFB
New Mexico
Attn: Capt. Marvin Atkins

Project Engineer /5561/ Comet 1
Rome Air Development Center
Griffiss AFB
New York
Attn: Mr. Phillip Sandler

Department of Electrical Engineering 1
New York University
University Heights
New York, New York
Attn: Mr. Thomas Henion

BMDR 8
Room 2B 263
The Pentagon
Washington 25, D. C.
Attn: Lt. Col. W. B. Lindsay

Mr. John Emmett 1
Physics Department
Stanford University
Palo Alto, California

Secretary, Special Group on Optical Masers 3
ODDRCE Advisory Group on Electron Devices
346 Broadway - 8th Floor
New York 13, New York

ASD /ASRCE-31/ 1
Wright-Patterson AFB, Ohio

Dr. W. Holloway 1
Sperry Rand Research Center
Sudbury, Massachusetts

Technical Area Manager /760B/ 1
Surveillance Electronic Systems Division
L. G. Hanscom AFB
Massachusetts
Attn: Major H. I. Jones, Jr.

Commanding Officer 1
U. S. Naval Ordnance Laboratory
Corona, California

Director 1
U. S. Army Engineering Research
and Development Laboratories
Fort Belvoir, Virginia
Attn: Technical Documents Center

Office of the Director of Defense 2
Defense Research and Engineering
Information Office Library Branch
Pentagon Building
Washington 25, D. C.

U. S. Army Research Office 2
Box CM, Duke Station
Durham, North Carolina

Defense Documentation Center 20
Cameron Station Building
Alexandria 14, Virginia

Director 6
U. S. Naval Research Laboratory
Technical Information Officer
Code 2000, Code 2021
Washington 25, D. C.

Commanding Officer 1
Office of Naval Research Branch Office
219 S Dearborn Street
Chicago, Illinois 60604

Commanding Officer 1
Office of Naval Research Branch Office
207 W. 24th St.
New York 11, New York 10011

Commanding Officer 1
Office of Naval Research Branch Office
1000 Geary Street
San Francisco, California 94109

Air Force Office of Scientific Research 1
Washington 25, D. C.

Director 1
National Bureau of Standards
Washington 25, D. C.

Director 1
Research Department
U. S. Naval Ordnance Laboratory
White Oak, Silver Spring, Md.

Commanding Officer 1
Office of Naval Research Branch Office
1030 East Green Street
Pasadena, California 91101

Commanding Officer 1
Office of Naval Research Branch Office
495 Summer Street
Boston 10, Mass.

U. S. Naval Radiological Defense Laboratory 1
/Code 941/
San Francisco, California 94135

Commanding Officer 1
U. S. Army Materials Research Agency
Attn: Technical Library
Watertown, Massachusetts 02172

Boulder Laboratories
National Bureau of Standards
Attn: Library
Boulder, Colorado — 1

Air Force Weapons Laboratory
Attn: Guenther WLRPT
Kirtland Air Force base
New Mexico — 1

Chief, Bureau of Naval Weapons
Department of the Navy
Washington 25, D. C.
Attn: J. M. Lee RMGA-81 — 1

Air Force Cambridge Research Laboratories
Attn: CRXL-R, Research Library
Lawrence G. Hanscom Field
Bedford, Massachusetts — 1

Battelle Memorial Institute
505 King Avenue
Columbus 1, Ohio
Attn: BMI-Defender — 1

Headquarters, USAELRDL
Fort Monmouth, New Jersey 07703
Attn: SELRA/SAR, NO-4, X, and PF — 1

Commander, U. S. Naval Ordnance Test Station
China Lake, California
Attn: Mr. G. A. Wilkins/Code 4041/ — 1

J. C. Almasi
General Electric Company
Advanced Technology Laboratories
Schnectady, N. Y. — 1

Prof. Rubin Braunstein
University of California
Department of Physics
Los Angeles 24, California — 1

N. I. Adams
Perkin-Elmer Corp.
Norwalk, Conn. 1

E. P. Reidel
Quantum Electronics Dept.
Westinghouse Electric Corp.
Research Laboratories
Pittsburgh, Pa. 1

Prof. H. G. Hanson
University of Minnesota
Duluth, Minn. 1

P. Schaffer
Lexington Laboratories, Inc.
84 Sherman St.
Cambridge, Mass. 1

L. E. Rautiola
Linde Company, Division of Union Carbide
East Chicago, Ind. 1

F. S. Galasso
United Aircraft Corp. Research Labs.
400 Main Street
East Hartford, Conn. 1

J. W. Nielson
Airtron, Division of Litton Industries
Morris Plains, N. J. 1

E. M. Flanigen
Linde Company
Division of Union Carbide
Tonawanda, N. Y. 1

W. Prindle
American Optical Company
14 Mechanic St.
Southbridge, Mass. 1

R. G. Meyerand 1
Plasma Physics
United Aircraft Corp.
East Hartford 8, Conn.

Prof. N. Bloembergen 1
Harvard University
Division of Engineering & Applied Physics
Cambridge 38, Mass.

Prof. R. J. Collins 1
University of Minnesota
Department of Electrical Eng.
Minneapolis 14, Minn.

Dr. Alan Kolb 1
U. S. Naval Research Lab.
Washington, D. C.

Prof. J. M. Feldman 1
Carnegie Institute of Technology
Department of Electrical Engr.
Pittsburgh 13, Pa.

Prof. Arthur Schawlow 1
Stanford University
Stanford, California

Research Materials Information Center 1
Oak Ridge National Laboratory
Post Office Box X
Oak Ridge, Tenn. 37831

J-5 Plans and Policy Directorate 1
Joint Chiefs of Staff
Requirements and Development Division
Attn: Special Projects Branch
Room 2D982, The Pentagon
Washington, D. C., 20301

Advanced Research Projects Agency 1
Research and Development Field Unit
APO 143, Box 41
San Francisco, California

Advanced Research Projects Agency 1
Research & Development Field Unit
APO 146, Box 271
San Francisco, California
Attn: Mr. Tom Brundage

Air Force Materials Laboratory 1
Air Force Systems Command
Wright-Patterson Air Force Base, Ohio 45433
Attn: MAAM (Lt. John H. Estess)

Dr. C. H. Church 1
Westinghouse Electric Corporation
Research Laboratories
Pittsburgh 35, Pennsylvania

Prof. Donald S. McClure 1
Institute for the Study of Metals
University of Chicago
Chicago 37, Illinois

Dr. Daniel Grafstein 1
General Precision, Inc.
Aerospace Group
Little Falls, New Jersey

Professor R. C. Ohlmann 1
Westinghouse Research Laboratories
Pittsburgh, Pennsylvania

Dr. R. C. Linares 1
Perkin-Elmer Corporation
Solid State Materials Branch
Norwalk, Connecticut 06852

Dr. J. G. Atwood 1
Perkin-Elmer Corporation
Electro-Optical Division
Norwalk, Connecticut

Prof. S. Claesson 1
Uppsala University
Uppsala, Sweden